Stereoselective Synthesis of [L-Arg-L/D-3-(2-naphthyl)alanine]-Type (*E*)-Alkene Dipeptide Isosteres and Its Application to the Synthesis and Biological Evaluation of Pseudopeptide Analogues of the CXCR4 Antagonist FC131

Hirokazu Tamamura,*,† Kenichi Hiramatsu,† Satoshi Ueda,† Zixuan Wang,‡ Shuichi Kusano,§ Shigemi Terakubo,§ John O. Trent,∥ Stephen C. Peiper,‡ Naoki Yamamoto,⊥ Hideki Nakashima,§ Akira Otaka,† and Nobutaka Fujii*,†

Graduate School of Pharmaceutical Sciences, Kyoto University, Sakyo-ku, Kyoto 606-8501, Japan, Medical College of Georgia, Augusta, Georgia 30912, St. Marianna University, School of Medicine, Miyamae-ku, Kawasaki 216-8511, Japan, James Graham Brown Cancer Center, University of Louisville, Louisville, Kentucky 40202, and Tokyo Medical and Dental University, School of Medicine, Bunkyo-ku, Tokyo 113-8519, Japan

Received July 18, 2004

L,L-Type and L,D-type (*E*)-alkene dipeptide isosteres (EADIs) that have unnatural side chains at the α-position were synthesized by the combination of stereoselective aziridinyl ring-opening reactions and organozinc−copper-mediated *anti*-S_N2' reactions toward a single substrate of γ,δ-*cis*-γ,δ-epimino (*E*)-α,β-enoate. The utility of this methodology was demonstrated by the stereoselective synthesis of a set of diastereomeric EADIs of L-Arg-L/D-3-(2-naphthyl)alanine (Nal) that is contained in a small CXCR4 antagonist FC131 [*cyclo*(-D-Tyr-Arg-Arg-Nal-Gly-)]. Furthermore, a (Nal-Gly)-type EADI was synthesized by samarium diiodide (SmI_2)-induced reduction of a γ-acetoxy-α,β-enoate. Several FC131 analogues, in which these EADIs were inserted for reduction of their peptide character, were synthesized with analogues containing reduced amide-type dipeptide isosteres to investigate the importance of these amide bonds for anti-HIV and CXCR4-antagonistic activity.

Introduction

The practical utility of (*E*)-alkene dipeptide isosteres (EADIs) has been intensively investigated in structure−activity relationship (SAR) studies of biologically active peptides toward development of peptide-lead drugs.[1−7] Backbone replacements of amide bonds in peptides by EADIs provide information on the contributions of the corresponding amide bonds on biological activity. We previously established a completely stereocontrolled synthetic process for L,L-type and L,D-type EADIs starting from L-amino acid.[8,9] As shown in Scheme 1, treatment of *N*-aryl-γ,δ-*cis*-γ,δ-epimino (*E*)-α,β-enoates (*cis*-(*E*)-enoates) **1** with methanesulfonic acid (MSA) gives γ-mesyloxy-α,β-enoates **2**, which can be converted into L,D-type EADIs **3** by organocopper-mediated α-alkylation via *anti*-S_N2' reactions, whereas organocopper treatment of *cis*-(*E*)-enoates **1** affords L,L-type EADIs **4**. However, this synthetic procedure has not yet been optimized, because it involves a potential limitation on the introduction of functional groups into the side chain (R^3) at the α-position. In a standard procedure, organocopper reagents, which were prepared by CuCN and RLi or RMgX (X = Cl or Br), are used for α-alkylation.[2,4] In the α-alkylation of the synthesis of (Xaa-L/D-Glu)-type EADIs,[10] organozinc−copper reagents are used, which are prepared from $IZnCH_2CH_2CO_2R$ and CuCN.[11−15] In this study, to demonstrate the general utility of organozinc−copper reagents, a set of EADIs of L-Arg-L/D-3-(2-naphthyl)alanine (Nal) were synthesized as model compounds via the γ,δ-*cis*-γ,δ-epimino (*E*)-α,β-enoate by the combination of MSA-mediated aziridinyl ring-opening reactions and α-alkylation with organozinc−copper reagents, which were prepared from 2-naphthylmethylZnBr and CuCN. The dipeptide sequence, Arg-Nal, is part of the low molecular weight CXCR4 antagonist, FC131, which was recently developed by us (Figure 1).[16]

Scheme 1[a]

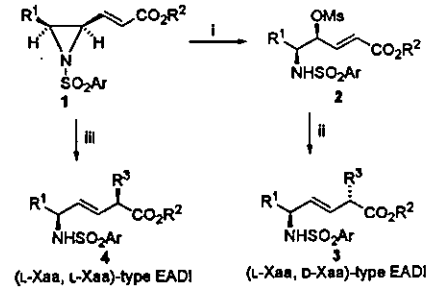

[a] R^1, R^2, R^3 = alkyl; Ar = 2,4,6-trimethylphenylsulfonyl (Mts) or Ts. Reagents: (i) MsOH; (ii) $R^3Cu(CN)MgX{\cdot}BF_3$ (X = Cl or Br) or $R^3Cu(CN)Li{\cdot}BF_3$; (iii) $R^3Cu(CN)MgX{\cdot}2LiX$ (X = Cl or Br) or $R^3Cu(CN)Li{\cdot}2LiX$.

In this study, to demonstrate the general utility of organozinc−copper reagents, a set of EADIs of L-Arg-L/D-3-(2-naphthyl)alanine (Nal) were synthesized as model compounds via the γ,δ-*cis*-γ,δ-epimino (*E*)-α,β-enoate by the combination of MSA-mediated aziridinyl ring-opening reactions and α-alkylation with organozinc−copper reagents, which were prepared from 2-naphthylmethylZnBr and CuCN. The dipeptide sequence, Arg-Nal, is part of the low molecular weight CXCR4 antagonist, FC131, which was recently developed by us (Figure 1).[16]

CXCR4 is a chemokine receptor, which is involved in cell progression and metastasis of several types of cancer,[17−19] HIV entry,[20] and rheumatoid arthritis.[21,22] Thus, several inhibitors directed against CXCR4 have been developed.[23−27] We previously found a highly potent CXCR4 antagonist, T140, which is a 14-mer

* Corresponding authors. Tel: +81 75 753 4551, Fax: +81 75 753 4570, E-mail: tamamura@pharm.kyoto-u.ac.jp; nfujii@pharm.kyoto-u.ac.jp.
† Kyoto University.
‡ Medical College of Georgia.
§ St. Marianna University.
∥ University of Louisville.
⊥ Tokyo Medical and Dental University.

10.1021/jm049429h CCC: $30.25
Published on Web 12/21/2004

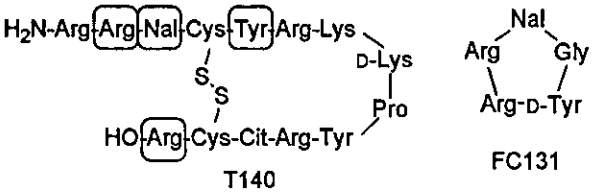

Figure 1. Structures of T140 and its downsized peptide FC131. Circled residues are the indispensable residues of T140 for the expression of strong CXCR4-antagonistic activity. Nal = L-3-(2-naphthyl)alanine, Cit = L-citrulline.

peptide with a disulfide bridge, and we identified four critical residues: Arg^2, Nal^3, Tyr^5, and Arg^{14} (Figure 1).[28-30] Molecular-size reduction of T140 based on the structural requirement led to the discovery of FC131, which has a cyclic pentapeptide template,[31-37] with CXCR4-antagonistic and anti-HIV activity comparable to those of T140.[16] We wish to investigate contributions of each amide bond in FC131 to the biological activity in order to develop pseudopeptides, in which the peptide character is reduced to obtain more druglike structures. For this purpose, EADIs and reduced amide-type dipeptide isosteres (RADIs) of Arg-Nal and Nal-Gly are required, because the amide bonds between Arg^2 and Nal^3 and between Nal^3 and Cys^4 were found to be cleaved by treatment of T140 analogues with rat liver homogenates.[38,39] Thus, (L-Arg-L/D-Nal)-type EADIs were synthesized in the study described here, and a (Nal-Gly)-type EADI was also synthesized by another method using the samarium diiodide (SmI_2)-induced reduction of a γ-acetoxy-α,β-enoate.[40,41] RADIs of Arg-Nal and Nal-Gly were prepared by a standard method of reductive amination. Then, several FC131 analogues, in which the above isosteres were introduced, were synthesized to identify the biological importance of these amide bonds.

Results and Discussion

Synthesis of (L-Arg-L/D-Nal)-Type EADIs. (L-Arg-L/D-Nal)-type EADIs were synthesized via the same key intermediate *N*-2-nitrobenzenesulfonyl (Ns)-γ,δ-*cis*-γ,δ-epimino (*E*)-α,β-enoate, **9**, as synthetic model compounds for the investigation of the feasibility of α-alkylation using organozinc−copper reagents as well as precursor dipeptide isosteres used for the synthesis of partial nonpeptide analogues of FC131 (Scheme 2). Boc-Arg(Mts)-OMe (Mts = 2,4,6-trimethylbenzenesulfonyl) **5** was treated successively with diisobutylaluminum hydride (DIBAL-H) and vinylmagnesium chloride (CH_2=CHMgCl) to give exclusively the *threo*-amino alcohol **6** (a separable mixture of allyl alcohol **6**/*erythro*-isomer of **6** = 12:1). N^{α}-Ns protection[42,43] after the cleavage of the N^{α}-Boc group of **6** with HCl/dioxane followed by successive treatments consisting of the Mitsunobu reaction,[44] ozonolysis, and the modified Horner−Wadsworth−Emmons olefination[45] afforded *cis*-(*E*)-enoate **9**. *Anti*-S_N2' reaction of **9** with an organozinc−copper reagent,[11-15] 2-naphthylmethylCu(CN)-ZnBr·2LiCl, afforded an L,L-type EADI **10**, in which a (2*R*)-2-naphthylmethyl side chain was incorporated at the α-position, stereoselectively in 83% yield (diastereoselection > 99:1 from NMR analysis). N^{α}-Fmoc substitution for the N^{α}-Ns group of **10** followed by selective deprotection of the benzyl ester using thioanisole/TFA afforded a desired EADI, Fmoc-L-Arg(Mts)-ψ[(*E*)-CH=CH]-L-Nal-OH, **12**. Alternatively, exposure of **9** to MSA/$CHCl_3$ afforded exclusively δ-aminated γ-mesyloxy-α,β-enoate **13** by regio- and stereoselective S_N2 ring-opening reaction at the γ-carbon of **9**. Mesylate **13** was successively treated by an organozinc−copper reagent, 2-naphthylmethylCu(CN)ZnBr·BF_3, to afford an L,D-type EADI **14**, in which a (2*S*)-2-naphthylmethyl side chain was incorporated at the α-position, stereoselectively via an *anti*-S_N2'mechanism in 67% yield (diastereoselection > 99:1 from NMR analysis). **14** was similarly converted into another desired EADI, Fmoc-L-Arg(Mts)-ψ[(*E*)-CH=CH]-D-Nal-OH, **16**. As such, α-alkylation of both a *cis*-(*E*)-enoate and its ring-opened product using organozinc−copper reagents was successfully performed in the synthesis of (L-Arg-L/D-Nal)-type EADIs. An *N*-Ns group could be used in this synthetic scheme as an orthogonal *N*-protecting (activating) group instead of an *N*-Mts or *N*-Ts group. Relative configurations of the allyl alcohols (**6** and its erythro isomer) were determined by comparative nuclear Overhauser effect (NOE) measurements of these oxazolidinone derivatives **17** and **18** (Scheme 2).[2] The (*E*)-geometry of the double bond in the synthesized EADIs was assigned based on the coupling constant of the two olefinic protons on ^{1}H NMR analysis.

Synthesis of (L-Nal-Gly)-Type EADI. An (L-Nal-Gly)-type EADI was synthesized as shown in Scheme 3. Boc-L-Nal-OMe **19** was treated sequentially with DIBAL-H and CH_2=CHMgCl to give a diastereomixture of allyl alcohol **20**. Acetylation of **20** followed by ozonolysis and the modified Horner−Wadsworth−Emmons olefination afforded a γ-acetoxy-α,β-unsaturated ester **22**. Acetate **22** was reduced with SmI_2−^{t}BuOH to yield an (L-Nal-Gly)-type EADI **23** in 95% yield,[40,41] followed by deprotection of the N^{α}-Boc group and *tert*-butyl ester with TFA and reprotection with an N^{α}-Fmoc group to afford the desired EADI, Fmoc-L-Nal-ψ[(*E*)-CH=CH]-Gly-OH, **24**.

Synthesis of RADIs of Arg-Nal and Nal-Gly. (L-Arg-L-Nal)- and (L-Nal-Gly)-type RADIs were prepared for comparative studies. As shown in Scheme 4, Arg- and Nal-derived Weinreb amides **25** and **29** were treated with DIBAL-H to afford the corresponding aldehyde derivatives. Subsequently, reductive amination of the aldehydes was performed by treatments with carboxy-protected amino acids in the presence of acetic acid and sodium triacetoxy borohydride [$NaBH(OAc)_3$] to afford secondary amines **26** and **30**, respectively.[46] Protection of the *sec*-amino groups with Cbz groups followed by deprotection of the N^{α}-Boc group and *tert*-butyl ester with TFA and reprotection with an N^{α}-Fmoc group afforded the desired RADIs, Fmoc-L-Arg(Mts)-ψ-[CH_2−N(Cbz)]-L-Nal-OH, **28**, and Fmoc-L-Nal-ψ[CH_2−N(Cbz)]-Gly-OH, **32**, respectively.

Synthesis of Cyclic Pseudopeptides. The protected peptide chains were constructed on a hydrazino resin **34** by Fmoc-based solid-phase synthesis using ^{t}Bu and 2,2,4,6,7-pentamethyldihydrobenzofuran-5-sulfonyl (Pbf) groups for side-chain protection of D-Tyr and Arg, respectively (Scheme 5). N^{α}-Fmoc-protected dipeptide isosteres, EADIs **12**, **16**, and **24** and RADIs **28** and **32**, were similarly condensed. In the synthesis of cyclic pseudopeptides, two steps of deprotection/cleavage were adopted to prevent guanidino groups of Arg from

Scheme 2[a]

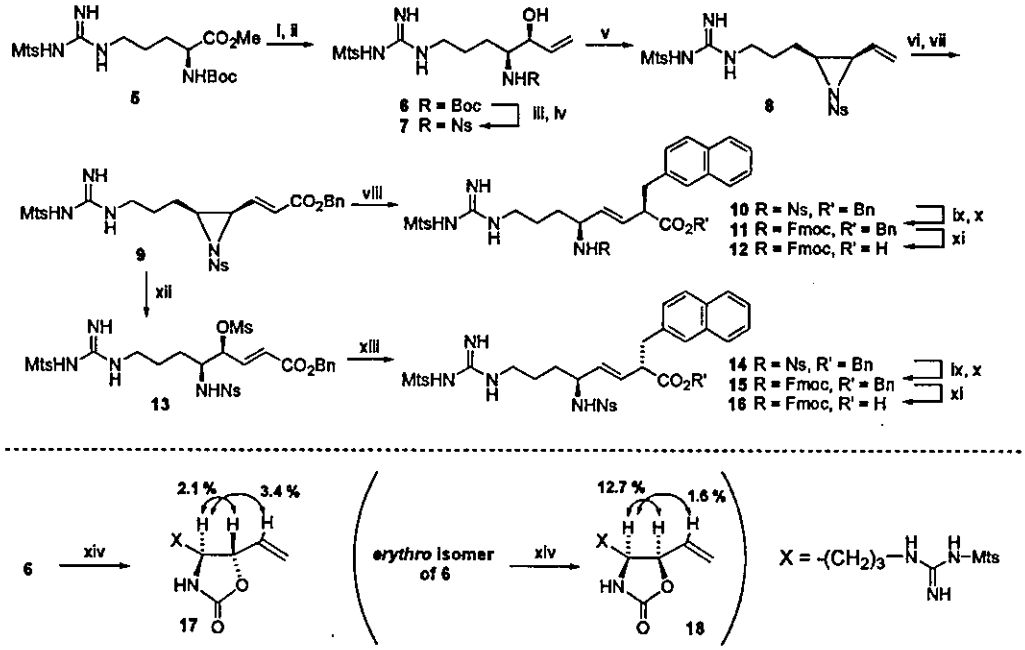

[a] Reagents: (i) DIBAL-H; (ii) CH_2=CHMgCl; (iii) HCl, anisole; (iv) Ns-Cl, pyridine; (v) Ph_3P, DEAD; (vi) O_3, then Me_2S; (vii) $(EtO)_2P(O)CH_2CO_2Bn$, LiCl, DIPEA; (viii) 2-naphthylmethylCu(CN)ZnBr·2LiCl; (ix) PhSH, K_2CO_3; (x) Fmoc-OSu, Et_3N; (xi) thioanisole, TFA; (xii) MsOH; (xiii) 2-naphthylmethylCu(CN)ZnBr·BF_3; (xiv) NaH.

Scheme 3[a]

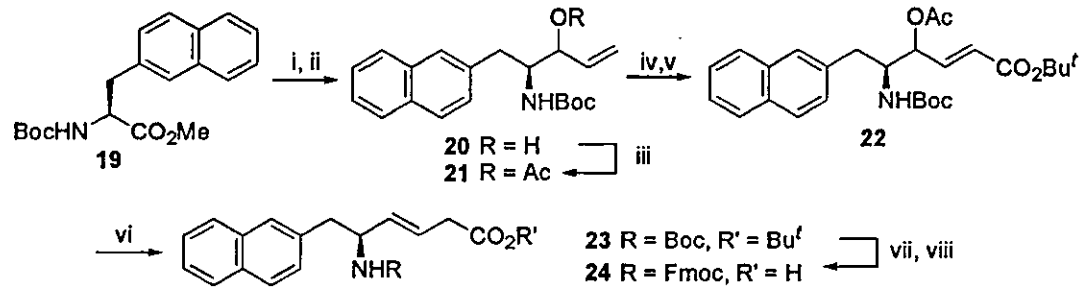

[a] Reagents: (i) DIBAL-H; (ii) CH_2=CHMgCl; (iii) Ac_2O, DMAP, pyridine; (iv) O_3, then Me_2S; (v) $(EtO)_2P(O)CH_2CO_2{}^tBu$, LiCl, DIPEA; (vi) SmI_2, ^tBuOH; (vii) anisole, TFA; (viii) Fmoc-OSu, Et_3N.

Scheme 4[a]

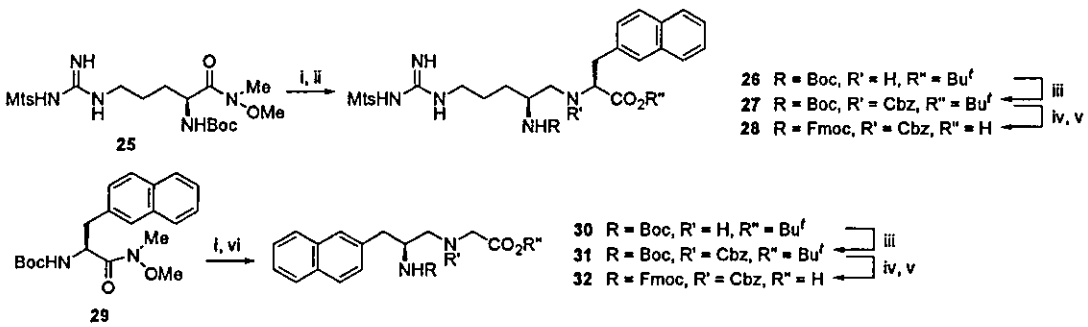

[a] Reagents: (i) DIBAL-H; (ii) H-Nal-O^{t}Bu, AcOH, $NaBH(OAc)_3$; (iii) Cbz-Cl, Et_3N; (iv) anisole, TFA; (v) Fmoc-OSu, Et_3N; (vi) H-Gly-O^{t}Bu, AcOH, $NaBH(OAc)_3$.

participating in cyclizing reaction as follows. After construction of peptide chains, pseudopeptide hydrazides **36** were obtained by cleavage from the resin **35** using 10% TFA/$CHCl_3$ without cleavage of Pbf, Mts, and Cbz groups (first deprotection). Cyclization of linear pseudopeptides by the azide procedure[47] in highly

Scheme 5[a]

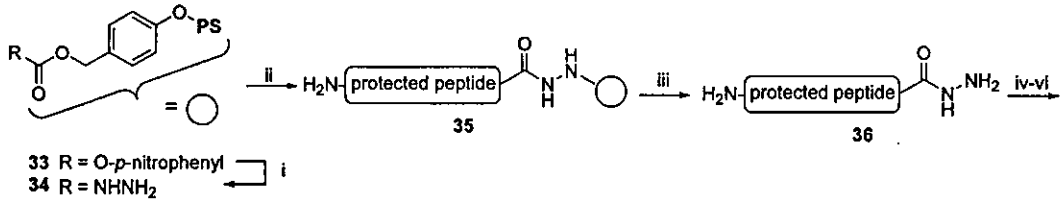

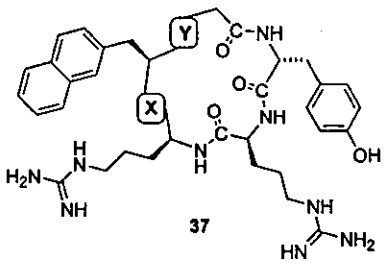

37

Compd.	Sequence (*cyclo*)	X	Y
FC131	(-D-Tyr-Arg-Arg-Nal-Gly-)	-CO-NH-	-CO-NH-
37a	(-D-Tyr-Arg-Arg-Nal-Gly-)	-CH=CH-	-CO-NH-
37b	(-D-Tyr-Arg-Arg-Nal-Gly-)	$-CH_2$-NH-	-CO-NH-
37c	(-D-Tyr-Arg-Arg-Nal-Gly-)	-CO-NH-	-CH=CH-
37d	(-D-Tyr-Arg-Arg-Nal-Gly-)	-CO-NH-	$-CH_2$-NH-
37e	(-D-Tyr-Arg-Arg-D-Nal-Gly-)	-CO-NH-	-CO-NH-
37f	(-D-Tyr-Arg-Arg-D-Nal-Gly-)	-CH=CH-	-CO-NH-

[a] Reagents: (i) NH_2NH_2·H_2O; (ii) Fmoc-based SPPS; (iii) TFA; (iv) HCl, isoamyl nitrite; (v) DIPEA; (vi) 1 M TMSBr–thioanisole/TFA, *m*-cresol, 1,2-ethanedithiol.

Table 1. Activity and Cytotoxicity of the Synthetic Compounds

compound (no.)	CC_{50}[a] (μM)	EC_{50}[b] (μM)	IC_{50}[c] (μM)
FC131	> 100	0.073	0.0045 ± 0.0018
37a	> 100	2.4	31–100[d]
37b	> 100	> 100	> 100
37c	> 100	2.4	0.18 ± 0.10
37d	> 100	0.98	0.032 ± 0.011
37e	> 100	1.9	0.19 ± 0.071
37f	> 100	9.1	21
T140	> 10	0.035	0.0039 ± 0.0004
AZT	57	0.018	

[a] CC_{50} values are based on the reduction of the viability of mock-infected MT-4 cells. Because the cytotoxicity of T140 was previously evaluated as CC_{50} > 40 μM, further estimation at high concentrations was omitted in this study. [b] EC_{50} values are based on the inhibition of HIV-induced cytopathogenicity in MT-4 cells. [c] IC_{50} values are based on the inhibition of [^{125}I]-SDF-1-binding to CXCR4 transfectants of CHO cells. All data are the mean values for at least three independent experiments. [d] **37a** showed significant antagonistic activity in 100 μM but hardly showed activity in 31 μM.

diluted dimethylformamide (DMF) solution followed by deprotection of Pbf, Mts, and Cbz groups with 1 M TMSBr–thioanisole/TFA (second deprotection) gave the desired cyclic pseudopeptides **37**.

Biological and Conformational Evaluation of Synthetic Cyclic Pseudopeptides. Anti-HIV activity based on the inhibition of HIV-1-induced cytopathogenicity in MT-4 cells was evaluated using the 3-(4,5-dimethylthiazol-2-yl)-2,5-diphenyltetrazolium bromide (MTT) method.[48] CXCR4-antagonistic activity was evaluated by the inhibition of [^{125}I]-SDF-1-binding to CXCR4 transfectants of CHO cells.[49] **37a**, an (L-Arg-L-Nal)-type EADI containing FC131 analogue, showed moderate anti-HIV activity (EC_{50} = 2.4 μM) and CXCR4-antagonistic activity (100 μM > IC_{50} > 31 μM). Introduction of an EADI into the Arg-Nal sequence caused a remarkable decrease in anti-HIV activity (33-fold lower activity). NMR and simulated annealing molecular dynamics (SA-MD) analysis of **37a** showed a pseudopeptide backbone structure with a nearly symmetrical pentagonal shape similar to that of FC131,[16] excluding the difference between the orientation of two protons in the (*E*)-alkene unit of **37a** and that of the carbonyl oxygen/amino proton in the Arg-Nal amide bond of FC131 (Figure 2a).[50] Substitution for the amide bond with the EADI caused an inversion of the olefinic plane (180° rotation of pseudo ψ and φ bonds), possibly due to dissolution of the 1,3-pseudo-allylic strain between the carbonyl group of Arg and the side chain of Nal. Introduction of an EADI into the Arg-D-Nal sequence of **37e** (an FC131 epimer, EC_{50} = 1.9 μM, IC_{50} = 190 nM) also caused a significant but moderate decrease in anti-HIV activity (the activity of **37f** is 5-fold lower than that of **37e**). The amide bonds of the Arg-L/D-Nal sequences were necessary for high potency. These results suggested that either a deletion of the hydrogen bond interaction with CXCR4 by the insertion of an EADI or an increase in hydrophobicity might be unsuitable. **37b**, an (L-Arg-L-Nal)-type RADI-containing FC131 analogue, did not show anti-HIV or CXCR4-antagonistic activity up to the concentration of 100 μM, suggesting that the planar nature of the amide bond is critical to maintain the pentagonal global conformation for high anti-HIV activity and that the replacement of the amide bond with RADI causes a conformational change of FC131. **37c**, an (L-Nal-Gly)-type EADI-containing FC131 analogue, showed almost the same anti-HIV activity (EC_{50} = 2.4 μM) as **37a** containing an (L-Arg-L-Nal)-type EADI. NMR and SA-MD analysis of **37c** showed a similar backbone structure with FC131 (Figure 2b).[50] The Nal-Gly amide bond was replaced by the EADI without an inversion of the olefinic plane. **37d**, an (L-Nal-Gly)-type RADI-containing FC131 analogue, exhibited relatively higher anti-HIV and CXCR4-antagonistic activities (EC_{50} = 0.98 μM, IC_{50} = 32 nM) than **37c** (IC_{50} = 180 nM), although these activities were weaker than those of FC131. These results also indicated an importance of the amide bond of the Nal-Gly sequence, as in the case of the Arg-Nal amide bond.

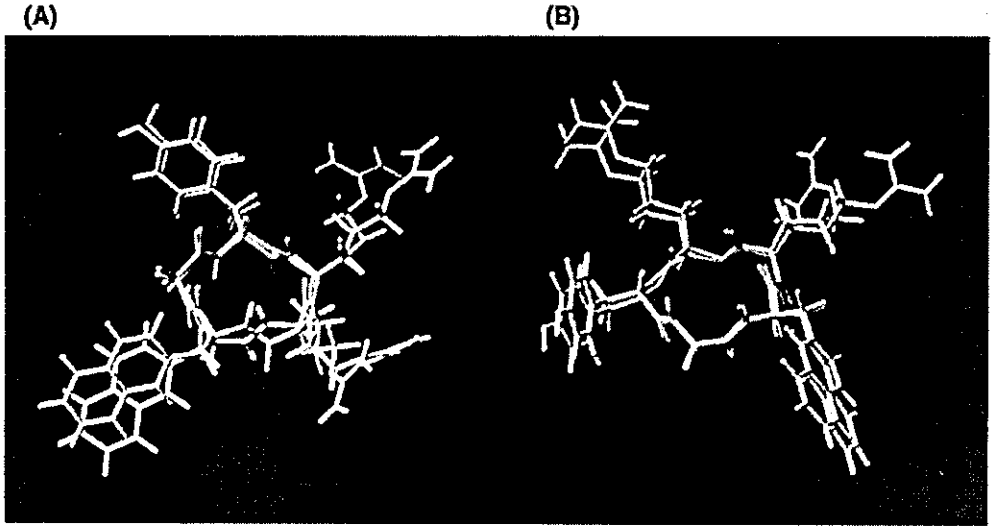

Figure 2. Superimpositions of low-energy structures of FC131 and **37a** (A) or **37c** (B). The FC131 structure is depicted in green, and the **37a** or **37c** structure is depicted in purple.

Conclusion

A set of (L-Arg-L/D-Nal)-type EADIs were synthesized from a single substrate of *γ,δ-cis-γ,δ*-epimino (*E*)-α,*β*-enoate by combination of MSA-mediated aziridinyl ring-opening reactions and *anti*-S_N2' reactions with organozinc−copper reagents that were prepared from 2-naphthylmethylZnBr and CuCN. Organozinc−copper-mediated α-alkylation reactions are thought to be useful for construction of several side chains at the α-position of EADIs, as organocopper-mediated α-alkylation reactions that have been generally used. Next, EADIs and RADIs of Arg-Nal and Nal-Gly, including the above EADIs, were synthesized and inserted into cyclic pentapeptides, FC131 analogues, to disclose biological importance of each amide bond. The present results will be useful for the development of nonpeptide CXCR4 antagonists derived from FC131. It is also noteworthy that EADI units were introduced into cyclic pentapeptides without any significant conformational changes in the pentagonal backbone structures, except for those of substituted (*E*)-alkene units, suggesting that the planar nature of (*E*)-alkene units caused the conformational maintenance of the backbones excluding the olefinic moiety. SA-MD analysis showed that the parent peptide (FC131) and the EADI-introduced pseudopeptides (**37a** and **37c**) have nearly equal distances between any two *β*-carbons in all of the side chains. It suggests that these compounds maintain similar dispositions of pharmacophores and that the biological differences between these compounds are derived from the (*E*)-alkene/amide bond units. As such, EADIs become useful tools for investigation of biological contributions of amide bonds.

Experimental Section

General. Melting points are uncorrected. ^{1}H NMR spectra were recorded using a JEOL EX-270, a JEOL AL-400, or a Bruker AM 600 spectrometer at 270, 400, or 600 MHz ^{1}H frequency in $CDCl_3$, respectively. Chemical shifts are reported in parts per million downfield from internal tetramethylsilane. Nominal (LRMS) and exact mass (HRMS) spectra were recorded on a JEOL JMS-01SG-2 or JMS-HX/HX 110A mass spectrometer. Ion-spray (IS)-mass spectrum was obtained with a Sciex API *III*E triple quadrupole mass spectrometer (Toronto, Canada). Optical rotations were measured in $CHCl_3$ or H_2O with a JASCO DIP-360 digital polarimeter (Tokyo, Japan) or a Horiba high-sensitive polarimeter SEPA-200 (Kyoto, Japan). For flash column chromatography, silica gel 60 H (silica gel for thin-layer chromatography, Merck) and Wakogel C-200 (silica gel for column chromatography) were employed. HPLC solvents were H_2O and MeCN, both containing 0.1% (v/v) TFA. For analytical HPLC, a Cosmosil 5C18-AR column (4.6 mm × 250 mm, Nacalai Tesque Inc., Kyoto, Japan) was eluted with a linear gradient of MeCN at a flow rate of 1 mL/min on a Waters model 600 (Nihon Millipore, Ltd., Tokyo, Japan). Preparative HPLC was performed on a Waters Delta Prep 4000 equipped with a Cosmosil 5C18-AR column (20 mm × 250 mm, Nacalai Tesque Inc.) using an isocratic mode of MeCN at a flow rate of 15 mL/min.

Boc-Arg(Mts)-OMe, 5. To a stirred solution of Boc-Arg(Mts)-OH (10.0 g, 21.9 mmol) in DMF (50 mL) at 4 °C were added potassium bicarbonate (4.39 g, 43.8 mmol) and methyl iodide (2.73 mL, 43.8 mmol), and the mixture was stirred at room temperature for 10 h. The reaction mixture was concentrated under reduced pressure. The residue was extracted with EtOAc, and the extract was washed successively with saturated citric acid, brine, saturated aqueous $NaHCO_3$, and brine and dried over $MgSO_4$. Concentration under reduced pressure gave 10.4 g (21.8 mmol, 100%) of methyl ester **5** as a yellow oil.

$[\alpha]^{22}_D$ −4.25 (*c* 0.47, $CHCl_3$). ^{1}H NMR (270 MHz, $CDCl_3$) *δ*: 1.42 (9H, s, *tert*-Bu), 1.61 (2H, br m, CH_2), 1.78 (2H, br m, CH_2), 2.59 (3H, s, Ar-*p*-Me), 2.66 (6H, s, Ar-*o*-Me), 3.22 (2H, br m, CH_2), 3.73 (3H, s, OMe), 4.21−4.28 (1H, m, CH), 5.23 (1H, d, J = 8.2 Hz, NH), 6.14 (3H, br, guanidino), 6.89 (2H, s, ArH). *m/z* (FAB-LRMS): 471 (MH^+), 415, 371, 289 (base peak), 119. Found (FAB-HRMS): 471.2268. Calcd for $C_{21}H_{35}O_6N_4S$ (MH^+): 471.2277.

***N-tert*-Butoxy-[2(*S*)-hydroxy-1(*S*)-[3-[[imino[[(2,4,6-trimethylphenyl)sulfonyl]amino]methyl]amino]propyl]but-3-enyl]formamide, 6.** To a stirred solution of Boc-Arg(Mts)-OMe, **5** (5.0 g, 10.6 mmol), in toluene/CH_2Cl_2 (1:1 (v/v) 100 mL) was added dropwise a solution of DIBAL-H in toluene (1.0 M, 32 mL, 32 mmol) at −50 °C under argon, and the mixture was stirred at −78 °C for 2 h. To the solution, was added dropwise a vinyl Grignard (CH_2=$CHMgCl$) reagent in THF (13 mL, 32 mmol) at −78 °C, and the mixture was stirred for 6 h with a gradual warming to 0 °C. The reaction was quenched with saturated aqueous citric acid at −78 °C, and organic solvents were concentrated under reduced pressure. The residue was extracted with EtOAc, and the extract was washed successively with saturated aqueous citric acid, satu-

rated aqueous $NaHCO_3$, and brine and dried over $MgSO_4$. Concentration under reduced pressure followed by flash column chromatography over silica gel with EtOAc/*n*-hexane (2:1) gave a *threo*-allyl alcohol **6** and an *erythro*-allyl alcohol (2*R* isomer of **6**) (12:1), in order of elution (**6**, 1.5 g, 30% yield from **5**).

Compound **6**: colorless oil. $[\alpha]^{22}_D$ −15.74 (*c* 0.63, $CHCl_3$). ^1H NMR (270 MHz, $CDCl_3$) δ: 1.40 (9H, s, *tert*-Bu), 1.57 (2H, br m, 2-CH_2), 1.70 (2H, br m, 1-CH_2), 2.26 (3H, s, Ar-*p*-Me), 2.66 (6H, s, Ar-*o*-Me), 3.24 (2H, br m, 3-CH_2), 3.55 (1H, br, 1-H), 4.08 (1H, br, 2-H), 4.97 (1H, d, J = 9.7 Hz, NH), 5.18 (1H, d, J = 10.5 Hz, C*H*H=), 5.28 (1H, d, J = 17.3 Hz, CH*H*=), 5.77−5.89 (1H, m, CH=), 6.20 (3H, br, guanidino), 6.89 (2H, s, ArH). *m/z* (ISMS): 469.5 (MH^+). Found (FAB-HRMS): 469.2490. Calcd for $C_{22}H_{37}O_5N_4S$ (MH^+): 469.2485.

Compound 2*R* isomer of **6**: colorless oil. $[\alpha]^{21}_D$ −4.57 (*c* 2.84, $CHCl_3$). ^1H NMR (270 MHz, $CDCl_3$) δ: 1.41 (9H, s, *tert*-Bu), 1.48 (2H, br m, 2-CH_2), 1.64 (2H, br m, 1-CH_2), 2.30 (3H, s, Ar-*p*-Me), 2.63 (6H, s, Ar-*o*-Me), 3.15 (2H, br m, 3-CH_2), 3.63 (1H, br, 1-H), 4.18 (1H, br, 2-H), 5.12 (1H, br, NH), 5.24 (1H, d, J = 10.5 Hz, C*H*H=), 5.32 (1H, d, J = 17.0 Hz, CH*H*=), 5.74−5.85 (1H, m, CH=), 6.32 (3H, br, guanidino), 6.95 (2H, s, ArH). *m/z* (ISMS): 469.5 (MH^+).

[2(*S*)-Hydroxy-1(*S*)-[3-[[imino[[(2,4,6-trimethylphenyl)-sulfonyl]amino]methyl]amino]propyl]but-3-enyl][(2-nitrophenyl)sulfonyl]amine, 7. To a mixture of allyl alcohol **6** (4.2 g, 9.0 mmol) and anisole (0.97 mL, 9.0 mmol) at 0 °C was added 4 M HCl/dioxane (100 mL), and the mixture was stirred at room temperature for 2 h. The mixture was concentrated under reduced pressure. To a stirred solution of the residue in $CHCl_3$ (20 mL) at 0 °C were added 2-nitrobenzenesulfonyl chloride (2.38 g, 10.8 mmol), triethylamine (Et_3N) (5 mL), and pyridine (20 mL), and the mixture was allowed to warm to room temperature, stirred at this temperature for 12 h, and extracted with $CHCl_3$. The extract was washed with saturated aqueous citric acid, saturated aqueous $NaHCO_3$, and brine and dried over $MgSO_4$. Concentration under reduced pressure followed by chromatography over silica gel with $CHCl_3$/MeOH (18:1) gave 3.2 g (5.8 mmol, 65% from **6**) of **7** as a yellow oil.

$[\alpha]^{23}_D$ −57.79 (*c* 1.83, $CHCl_3$). ^1H NMR (270 MHz, $CDCl_3$) δ: 1.61 (4H, br m, 1, 2-CH_2), 2.27 (3H, s, Ar-*p*-Me), 2.64 (6H, s, Ar-*o*-Me), 3.15 (2H, br m, 3-CH_2), 3.50 (1H, br, 1-H), 3.72−3.78 (1H, m, 2-H), 4.72 (1H, d, J = 10.5 Hz, C*H*H=), 5.07 (1H, d, J = 17.0 Hz, CH*H*=), 5.42−5.48 (1H, m, CH=), 5.90 (1H, d, J = 8.1 Hz, NH), 6.26 (3H, br, guanidino), 6.90 (2H, s, ArH), 7.65−7.69 (2H, m, ArH), 7.78−7.82 (1H, m, ArH), 8.04−8.08 (1H, m, ArH). *m/z* (ISMS): 554.5 (MH^+). Found (FAB-HRMS): 554.1735. Calcd for $C_{23}H_{32}O_7N_5S_2$ (MH^+): 554.1743.

3(*S*)-[3-[[Imino[[(2,4,6-trimethylphenyl)sulfonyl]amino]methyl]amino]propyl]-1-[(2-nitrophenyl)sulfonyl]-2(*R*)-vinylaziridine, 8. To a stirred solution of allyl alcohol **7** (3.1 g, 5.6 mmol) in dry THF (30 mL) at 0 °C were added triphenylphosphine (1.6 g, 6.2 mmol) and diethyl azodicarbonate (2.4 mL of a 40% solution in toluene, 6.2 mmol), and the reaction mixture was stirred at this temperature for 30 min. The mixture was concentrated under reduced pressure and purified by chromatography over silica gel with EtOAc/*n*-hexane (2:1) to give 2.8 g (5.2 mmol, 93% yield from **7**) of aziridine **8** as a yellow oil.

$[\alpha]^{23}_D$ −10.45 (*c* 2.20, $CHCl_3$). ^1H NMR (270 MHz, $CDCl_3$) δ: 1.48 (4H, br m, 1, 2-CH_2), 2.26 (3H, s, Ar-*p*-Me), 2.65 (6H, s, Ar-*o*-Me), 3.02 (1H, br, 2-H), 3.15 (2H, br m, 3-CH_2), 3.46 (1H, br, 3-H), 5.29 (1H, d, J = 9.7 Hz, C*H*H=), 5.42 (1H, d, J = 17.0 Hz, CH*H*=), 5.45−5.53 (1H, m, CH=), 6.41 (3H, br, guanidino), 6.88 (2H, s, ArH), 7.45−7.50 (2H, m, ArH), 7.54−7.75 (2H, m, ArH). *m/z* (ISMS): 536.5 (MH^+). Found (FAB-HRMS): 536.1630. Calcd for $C_{23}H_{30}O_6N_5S_2$ (MH^+): 536.1638.

Phenylmethyl 3-3(*S*)-[3-[[Imino[[(2, 4, 6-trimethylphenyl)sulfonyl]amino]methyl]amino]propyl]-2(*R*)-[(2-nitrophenyl)sulfonyl-2-aziridinyl]prop-2-enoate, 9. To a solution of aziridine **8** (1.2 g, 2.2 mmol) in CH_2Cl_2 (30 mL) was bubbled O_3 gas at −78 °C until a blue color persisted. To the above solution was added Me_2S (1.7 mL, 22 mmol), and the mixture was stirred for 30 min and then dried over $MgSO_4$. Concentration under reduced pressure gave an oily residue of a crude aldehyde, which was used immediately in the next step without further purification. To a stirred suspension of LiCl (230 mg, 5.4 mmol) in MeCN (5 mL) under argon, were added $(EtO)_2P(O)CH_2CO_2Bn$ (1.5 mL, 5.4 mmol) and $(^iPr)_2NEt$ (DIPEA) (0.94 mL, 5.4 mmol) at 0 °C. After 20 min, the above aldehyde in MeCN (15 mL) was added to the mixture at 0 °C, and the mixture was stirred at this temperature for 8 h. The mixture was concentrated under reduced pressure, and the residue was extracted with EtOAc. The extract was washed successively with saturated aqueous citric acid and H_2O and dried over $MgSO_4$. Concentration under reduced pressure followed by chromatography over silica gel with $CHCl_3$/MeOH (40:1) gave the title compound **9** (1.0 g, 1.5 mmol, 67% yield from **8**) as a colorless oil.

$[\alpha]^{23}_D$ −10.1 (*c* 1.49, $CHCl_3$). ^1H NMR (270 MHz, $CDCl_3$) δ: 1.63 (4H, br m, 1, 2-CH_2), 2.17 (3H, s, Ar-*p*-Me), 2.64 (6H, s, Ar-*o*-Me), 3.20 (2H, br m, 3-CH_2), 3.22 (1H, br, 2-H), 3.61 (1H, br, 3-H), 5.15 (2H, s, CH_2), 6.18 (1H, dd, J = 15.7, 0.8 Hz, CH=), 6.22 (3H, br, guanidino), 6.66 (1H, dd, J = 15.5, 6.9 Hz, CH=), 6.88 (2H, s, ArH), 7.34 (5H, s, ArH), 7.56−7.60 (1H, m, ArH), 7.71−7.79 (2H, m, ArH), 8.13−8.17 (1H, m, ArH). *m/z* (ISMS): 670.5 (MH^+). Found (FAB-HRMS): 670.2019. Calcd for $C_{31}H_{36}O_8N_5S_2$ (MH^+): 670.2005.

Phenylmethyl 8-[[Imino[[(2,4,6-trimethylphenyl)sulfonyl]amino]methyl]amino]-5(*S*)-[[(2-nitrophenyl)sulfonyl]amino]-2(*R*)-(naphthylmethyl)oct-3-enoate [Ns-L-Arg-(Mts)-ψ[(*E*)-CH=CH]-L-Nal-OBn], 10. To a stirred solution of CuCN (219 mg, 2.45 mmol) and LiCl (207 mg, 4.89 mmol) in dry THF (3.0 mL) under argon at −78 °C, was added dropwise 0.5 M (2-naphthylmethyl)zincbromide in THF solution (4.9 mL, 2.45 mmol), and the mixture was stirred at 0 °C for 10 min. A solution of enoate **9** (273 mg, 0.408 mmol) in dry THF (9.0 mL) was added dropwise to the above mixture at −78 °C with stirring, and the stirring was continued for 30 min followed by quenching with 10 mL of a 1:1 saturated aqueous NH_4Cl/28% NH_4OH solution. The mixture was extracted with Et_2O, and the extract was washed with saturated aqueous NH_4Cl and brine and dried over $MgSO_4$. Concentration under reduced pressure gave an oily residue, which was purified by chromatography over silica gel with *n*-hexane/EtOAc (1:2) to yield 273 mg (0.337 mmol, 83% yield from **9**) of compound **10** as a yellow oil. $[\alpha]^{33}_D$ −80.9 (*c* 0.61, $CHCl_3$). ^1H NMR (270 MHz, $CDCl_3$) δ: 1.35 (2H, br m, 2-CH_2), 1.55 (2H, br m, 1-CH_2), 2.04 (3H, s, Ar-*p*-Me), 2.26 (6H, s, Ar-*o*-Me), 2.97 (2H, br, CH_2), 2.98 (2H, br m, 3-CH_2), 3.20−3.25 (1H, m, 2-H), 3.90 (1H, br, 5-H), 4.93 (2H, s, CH_2), 5.24 (1H, dd, J = 15.5, 6.9 Hz, CH=), 5.50 (1H, dd, J = 15.4, 8.4 Hz, CH=), 5.67 (1H, d, J = 4.6 Hz, NH), 5.95 (3H, br, guanidino), 6.89 (2H, s, ArH), 7.05−7.28 (7H, m, ArH), 7.42−7.77 (9H, m, ArH), 7.96−8.00 (1H, m, ArH). *m/z* (ISMS): 814.0 (MH^+). Found (FAB-HRMS): 812.2803. Calcd for $C_{42}H_{46}O_8N_5S_2$ (MH^+): 812.2788.

Phenylmethyl 5(*S*)-[(Fluoren-9-ylmethoxy)carbonylamino]-8-[[imino[[(2,4,6-trimethylphenyl)sulfonyl]amino]methyl]amino]-2(*R*)-(2-naphthylmethyl)oct-3-enoate [Fmoc-L-Arg(Mts)-ψ[(*E*)-CH=CH]-L-Nal-OBn], 11. To a stirred solution of enoate **10** (81 mg, 0.10 mmol) in DMSO/MeCN (1:49, 5 mL), were added thiophenol (31 μL, 0.3 mmol) and K_2CO_3 (55 mg, 0.4 mmol) at room temperature, and the mixture was stirred at 50 °C for 1 h. The solution was filtered, and the filtrate was concentrated under reduced pressure. The residue was extracted with EtOAc, washed with brine, and dried over $MgSO_4$. Concentration under reduced pressure gave an oily residue, which was dissolved in THF/H_2O (1:1, 50 mL). Fmoc-OSu (33 mg, 0.1 mmol) and Et_3N (27 μL, 0.19 mmol) were added to the above solution at 0 °C. After being stirred for 6 h, the mixture was acidified with 0.1 M HCl and then extracted with EtOAc. The extract was washed with 0.1 M HCl and brine and dried over $MgSO_4$. Concentration under reduced pressure followed by chromatography over silica gel with *n*-hexane/EtOAc (1:2) gave the title compound **11** (60 mg, 70.9 μmol, 71% yield from **10**) as a colorless oil.

$[\alpha]^{29}_D$ −11.2 (*c* 0.63, $CHCl_3$). ^1H NMR (270 MHz, $CDCl_3$) δ: 1.26 (4H, br m, 1, 2-CH_2), 2.18 (3H, s, Ar-*p*-Me), 2.63 (6H, s,

Ar-*o*-Me), 2.94 (2H, br, CH_2), 3.19 (2H, br m, 3-CH_2), 3.38 (1H, br, 2-H), 3.96 (1H, br, 5-H), 4.12 (1H, t, J = 5.8 Hz, ArH), 4.35 (2H, t, J = 5.94 Hz, CH_2), 4.82 (1H, br, NH), 5.01 (2H, s, CH_2), 5.24 (1H, dd, J = 15.0, 5.7 Hz, CH=), 5.64 (1H, dd, J = 14.4, 7.8 Hz, CH=), 6.16 (3H, br, guanidino), 6.81 (2H, s, ArH), 7.08–7.28 (8H, m, ArH), 7.33–7.42 (4H, m, ArH), 7.42–7.54 (3H, m, ArH), 7.64–7.74 (5H, m, ArH). *m/z* (ISMS): 850.0 (MH^+). Found (FAB-HRMS): 849.3664. Calcd for $C_{51}H_{53}O_6N_4S_2$ (MH^+): 849.3686.

5(*S*)-[(Fluoren-9-ylmethoxy)carbonylamino]-8-[[imino-[[(2, 4, 6-trimethylphenyl)sulfonyl]amino]methyl]amino]-2(*R*)-(2-naphthylmethyl)oct-3-enoic Acid [Fmoc-L-Arg-(Mts)-ψ[(*E*)-CH=CH]-L-Nal-OH], 12. The enoate **11** (30 mg, 0.037 mmol) was dissolved in TFA (10 mL), and thioanisole (500 μL), *m*-cresol (200 μL), and 1,2-ethanedithiol (100 μL) were added to the solution at 0 °C, and the mixture was stirred for 12 h at room temperature. The mixture was concentrated under reduced pressure and extracted with EtOAc. The extract was washed with brine and dried over $MgSO_4$. Concentration under reduced pressure followed by chromatography over silica gel with *n*-hexane/EtOAc (1:4) gave the title compound **12** (28 mg, 0.036 mmol, 98% yield from **11**) as a colorless oil.

$[\alpha]^{23}_D$ −15.2 (*c* 0.07, $CHCl_3$). ^1H NMR (600 MHz, $CDCl_3$) δ: 1.25 (4H, br m, 1, 2-CH_2), 2.20 (3H, s, Ar-*p*-Me), 2.62 (6H, s, Ar-*o*-Me), 2.86 (2H, br, CH_2), 3.05 (2H, br m, 3-CH_2), 3.49 (1H, br, 2-H), 3.68 (1H, br, 5-H), 4.10 (1H, br, ArH), 4.20–4.26 (2H, m, CH_2), 4.93 (1H, br, CH=), 5.34 (1H, br, CH=), 5.38 (1H, br, NH), 5.95 (3H, br, guanidino), 6.84 (2H, s, ArH), 7.20–7.41 (7H, m, ArH), 7.48–7.57 (3H, m, ArH), 7.65–7.77 (5H, m, ArH). *m/z* (ISMS): 760.0 (MH^+). Found (FAB-HRMS): 759.3228. Calcd for $C_{44}H_{47}O_6N_4S_2$ (MH^+): 759.3216.

Phenylmethyl 8-[[Imino[[(2, 4, 6-trimethylphenyl)sulfonyl]amino]methyl]amino]-5(*S*)-[[(2-nitrophenyl)-sulfonyl]amino]-2(*S*)-(naphthylmethyl)oct-3-enoate [Ns-L-Arg(Mts)-ψ[(*E*)-CH=CH]-D-Nal-OBn], 14. To a stirred solution of enoate **9** (500 mg, 0.75 mmol) in $CHCl_3$ (5 mL) was added dropwise MSA (435 μL, 6.7 mmol) at room temperature with stirring, and the stirring was continued for 20 min. The mixture was extracted with EtOAc, and the extract was washed successively with aqueous 5% citric acid, water, aqueous 5% $NaHCO_3$, and water and dried over $MgSO_4$. Concentration under reduced pressure gave an oily residue of the crude mesylate **13**, which was used directly in the following step without further purification. To a stirred slurry of CuCN (269 mg, 3.0 mmol) in dry THF (5 mL) under argon at −78 °C was added dropwise (2-naphthylmethyl)zincbromide in THF solution (6.0 mL, 3.0 mmol), and the mixture was stirred at 0 °C for 15 min followed by addition of BF_3·Et_2O (369 μL, 3.0 mmol) at −78 °C and then stirred at −78 °C for 15 min. To the mixture at −78 °C with stirring was added by syringe a solution of the crude mesylate **13** in THF (10 mL), and the stirring was continued at −78 °C for 1 h followed by quenching with saturated aqueous NH_4Cl and aqueous 28% NH_4OH (1:1) at 0 °C. The mixture was allowed to warm to room temperature and extracted with Et_2O. The extract was washed with H_2O, dried over $MgSO_4$, and concentrated under reduced pressure. The residue was purified by chromatography over silica gel with *n*-hexane/EtOAc (1:2) to give 408 mg (0.50 mmol, 67% from **9**) of protected EADI **14** as a yellow oil. $[\alpha]^{32}_D$ −41.7 (*c* 0.60, $CHCl_3$). ^1H NMR (270 MHz, $CDCl_3$) δ: 1.54 (4H, br m, 1, 2-CH_2), 2.25 (3H, s, Ar-*p*-Me), 2.66 (6H, s, Ar-*o*-Me), 2.86 (2H, br m, 3-CH_2), 2.98–3.06 (2H, m, CH_2), 3.15–3.23 (1H, m, 2-H), 3.78–3.88 (1H, m, 5-H), 4.98 (2H, s, CH_2), 5.09 (1H, dd, J = 15.5, 8.0 Hz, CH=), 5.49 (1H, dd, J = 15.5, 8.2 Hz, CH=), 5.57 (1H, d, J = 8.4 Hz, NH), 6.09 (3H, br, guanidino), 6.89 (2H, s, ArH), 7.10–7.26 (7H, m, ArH), 7.37–7.76 (9H, m, ArH), 7.95–7.98 (1H, m, ArH). *m/z* (ISMS): 814.0 (MH^+). Found (FAB-HRMS): 812.2775. Calcd for $C_{42}H_{46}O_8N_5S_2$ (MH^+): 812.2788.

Phenylmethyl 5(*S*)-[(Fluoren-9-ylmethoxy)carbonyl-amino]-8-[[imino[[(2,4,6-trimethylphenyl)sulfonyl]amino]methyl]amino]-2(*S*)-(2-naphthylmethyl)oct-3-enoate [Fmoc-L-Arg(Mts)-ψ[(*E*)-CH=CH]-D-Nal-OBn], 15. By use of a procedure identical with that described for the preparation of **11** from **10**, the enoate **14** (30 mg, 37 μmol) was converted into 28 mg (36 μmol, 98% yield from **14**) of the title compound **15** as a colorless oil.

$[\alpha]^{29}_D$ −1.6 (*c* 0.61, $CHCl_3$). ^1H NMR (270 MHz, $CDCl_3$) δ: 1.14–1.30 (4H, br m, 1, 2-CH_2), 2.17 (3H, s, Ar-*p*-Me), 2.62 (6H, s, Ar-*o*-Me), 2.91 (2H, br m, 3-CH_2), 3.15–3.23 (2H, m, CH_2), 3.40 (1H, br, 2-H), 3.95 (1H, br, 5-H), 4.11 (1H, t, J = 6.5 Hz, ArH), 4.33 (2H, d, J = 5.7 Hz, CH_2), 4.85 (1H, d, J = 6.8 Hz, NH), 5.00 (2H, s, CH_2), 5.25 (1H, dd, J = 16.7, 6.8 Hz, CH=), 5.61 (1H, dd, J = 14.3, 7.6 Hz, CH=), 6.13 (3H, br, guanidino), 6.81 (2H, s, ArH), 7.09–7.27 (8H, m, ArH), 7.32–7.45 (4H, m, ArH), 7.46–7.56 (3H, m, ArH), 7.64–7.73 (5H, m, ArH). *m/z* (ISMS): 850.0 (MH^+). Found (FAB-HRMS): 849.3698. Calcd for $C_{51}H_{53}O_6N_4S_2$ (MH^+): 849.3686.

5(*S*)-[(Fluoren-9-ylmethoxy)carbonylamino]-8-[[imino-[[(2, 4, 6-trimethylphenyl)sulfonyl]amino]methyl]amino]-2(*S*)-(2-naphthylmethyl)oct-3-enoic Acid [Fmoc-L-Arg-(Mts)-ψ[(*E*)-CH=CH]-D-Nal-OH], 16. By use of a procedure identical with that described for the preparation of **12** from **11**, the enoate **15** (153 mg, 0.19 mmol) was converted into 144 mg (0.19 mmol, 99% yield from **15**) of the title compound **16** as a colorless oil.

$[\alpha]^{23}_D$ 10.8 (*c* 0.19, $CHCl_3$). ^1H NMR (270 MHz, $CDCl_3$) δ: 1.24 (4H, br m, 1, 2-CH_2), 2.17 (3H, s, Ar-*p*-Me), 2.70 (6H, s, Ar-*o*-Me), 2.90 (2H, br m, 3-CH_2), 3.07 (2H, m, CH_2), 3.29 (1H, br, 2-H), 3.67 (1H, br, 5-H), 4.06 (1H, t, J = 8.2 Hz, ArH), 4.28 (2H, d, J = 5.9 Hz, CH_2), 5.12 (1H, d, J = 5.9 Hz, NH), 5.26 (1H, dd, J = 15.0, 5.8 Hz, CH=), 5.59 (1H, dd, J = 15.0, 8.0 Hz, CH=), 6.19 (3H, br, guanidino), 6.80 (2H, s, ArH), 7.18–7.40 (7H, m, ArH), 7.46–7.54 (3H, m, ArH), 7.59–7.70 (5H, m, ArH). *m/z* (ISMS): 760.0 (MH^+). Found (FAB-HRMS): 759.3201. Calcd for $C_{44}H_{47}O_6N_4S_2$ (MH^+): 759.3216.

H-D-Tyr(O^{t}Bu)-Arg(Pbf)-Arg(Mts)-ψ[(*E*)-CH=CH]-Nal-Gly-NHNHCO−Wang Resin. *p*-Nitrophenyl carbonate Wang resin **33** (Calbiochem-Novabiochem Japan, Ltd., Tokyo, Japan, 0.93 mmol/g, 323 mg, 0.3 mmol) was treated with NH_2NH_2·H_2O (146 μL, 3.0 mmol) in DMF (3 mL) at room temperature for 2 h to give a hydrazide linker **34**. Protected peptide−resins were manually constructed by Fmoc-based solid-phase peptide synthesis. ^{t}Bu for Tyr and Mts or Pbf for Arg were employed for side-chain protection. Fmoc deprotection was achieved by 20% piperidine in DMF (1 min × 2 and 15 min × 1). Fmoc−amino acids including EADIs or RADIs were condensed to free amino groups by treatment with 3 equiv of reagents (Fmoc−amino acid, *N,N'*-diisopropylcarbodiimide (DIPCDI) and HOBt·H_2O) in DMF for 1.5 h.

***cyclo*(-D-Tyr-Arg-Arg-ψ[(*E*)-CH=CH]-Nal-Gly-)·2TFA (37a).** The protected **37a** resin (34 mg, 0.025 mmol) was treated with TFA (0.5 mL) in $CHCl_3$ (4.5 mL) at room temperature for 2 h, and the mixture was filtered. Concentration of the filtrate under reduced pressure gave a crude hydrazide (H-D-Tyr-Arg(Pbf)-Arg(Mts)-ψ[(*E*)-CH=CH]-Nal-Gly-$NHNH_2$) as a colorless powder. To a stirred solution of the hydrazide in DMF (1 mL) were added a solution of 4 M HCl in DMF (16.6 μL, 75 μmol) and isoamyl nitrite (40 μL, 0.20 mmol) at −30 °C. After being stirred at −10 °C for 20 min, the mixture was diluted with precooled DMF (50 mL). To the above solution was added DIPEA (191 μL, 1.1 mmol) at −30 °C, and the mixture was stirred for 48 h at −20 °C. Concentration under reduced pressure gave a yellow oil (crude *cyclo*(-D-Tyr-Arg(Pbf)-Arg(Mts)-ψ[(*E*)-CH=CH]-Nal-Gly-)). To the protected cyclic peptide were added *m*-cresol (0.4 mL, 3.6 mmol), 1, 2-ethanedithiol (160 μL, 1.9 mmol), thioanisole (1.0 mL, 8.5 mmol), TFA (10 mL), and bromotrimethylsilane (1.2 mL, 9.1 mmol) at 0 °C, and the stirring was continued at room temperature for 12 h. Concentration under reduced pressure and purification by preparative HPLC gave the cyclic pseudo-peptide **37a** (8.5 mg, 36% yield from protected **37a** resin) as a freeze-dried powder.

$[\alpha]^{27}_D$ −53.3 (*c* 0.24, H_2O). t_R = 28.6 min (linear gradient of MeCN in H_2O, 10 to 40% over 30 min). *m/z* (ISMS): 714.0 (MH^+). Found (FAB-HRMS): 713.3879. Calcd for $C_{37}H_{49}O_5N_{10}$ (MH^+): 713.3887.

***cyclo*(-D-Tyr-Arg-Arg-ψ[(*E*)-CH=CH]-D-Nal-Gly-)·2TFA (37f).** By use of a procedure identical with that described

for the preparation of **37a**, the protected **37f** (34 mg, 0.025 mmol) was converted into 9.8 mg (10.5 μmol, 42%) of the title compound **37f**, as a freeze-dried powder.

$[\alpha]^{26}_D$ −32.0 (*c* 0.13, H_2O). t_R = 28.9 min (linear gradient of MeCN in H_2O, 10 to 40% over 30 min). *m/z* (ISMS): 714.0 (MH^+). Found (FAB-HRMS): 713.3903. Calcd for $C_{37}H_{49}O_5N_{10}$ (MH^+): 713.3887.

(*tert*-Butoxy)-*N*-[2(*R,S*)-hydroxy-1(*S*)-(2-naphthylmethyl)but-3-enyl]formamide, 20. To a stirred solution of Boc-Nal-OMe **19** (4.0 g, 12.2 mmol) in CH_2Cl_2 (100 mL) was added dropwise a solution of DIBAL-H in toluene (1.0 M, 24.4 mL, 24.4 mmol) at −78 °C under argon, and the mixture was stirred at −78 °C for 2 h. To the solution was added dropwise a vinyl Grignard (CH_2=CHMgCl) reagent in THF (12.6 mL, 36.6 mmol) at −78 °C, and the mixture was stirred for 6 h with warming to 0 °C. The reaction was quenched with saturated aqueous citric acid at −78 °C, and organic solvents were concentrated under reduced pressure. The residue was extracted with EtOAc, and the extract was washed successively with saturated aqueous citric acid, saturated aqueous $NaHCO_3$, and brine and dried over $MgSO_4$. Concentration under reduced pressure followed by chromatography over silica gel with EtOAc/*n*-hexane (3:1) gave a mixture of *threo*- and *erythro*-allyl alcohols **20** (1.4 g, 35% yield from **19**) as a colorless oil. The mixture of diastereoisomer was used in the following step without further purification.

^{1}H NMR (270 MHz, $CDCl_3$) δ: 1.24−1.36 (9H, br, *tert*-Bu), 2.90−2.94 (1H, br, 2-H), 3.00−3.03 (2H, br, CH_2), 3.86−3.94 (1H, br, 1-H), 4.95−5.01 (1H, br, NH), 5.13−5.17 (1H, m, C*H*H=), 5.22−5.29 (1H, m, CH*H*=), 5.82−5.94 (1H, m, CH=), 7.38−7.43 (3H, m, ArH), 7.68−7.80 (4H, m, ArH). *m/z* (ISMS): 328.5 (MH^+). Found (FAB-HRMS): 328.1921. Calcd for $C_{20}H_{26}O_3N$ (MH^+): 328.1913.

1(*S*)-[1-[(*tert*-Butoxy)carbonylamino]-2-(naphthyl)ethyl]prop-2(*R, S*)-enyl Acetate, 21. To a stirred solution of allyl alcohol **20** (8.5 g, 26.0 mmol) in $CHCl_3$ (10 mL), were added acetic anhydride (11.0 mL, 117 mmol) and pyridine (18.9 mL, 234 mmol) at 4 °C, and the mixture was stirred at room temperature for 6 h. The mixture was concentrated under reduced pressure. The residue was extracted with EtOAc, and the extract was washed with aqueous 5% $NaHCO_3$, aqueous 1 M HCl, and brine and dried over $MgSO_4$. Concentration under reduced pressure followed by chromatography over silica gel with EtOAc/*n*-hexane (2:1) gave acetates **21** (5.7 g, 59% yield from **20**) as a colorless oil.

^{1}H NMR (270 MHz, $CDCl_3$) δ: 1.29−1.37 (9H, br, *tert*-Bu), 2.06−2.08 (3H, br, Me), 2.80−2.84 (1H, br, 2-H), 2.89−2.95 (2H, br, CH_2), 4.14−4.20 (1H, br, 1-H), 4.74−4.78 (1H, br, NH), 5.20−5.24 (1H, br m, C*H*H=), 5.25−5.30 (1H, br m, CH*H*=), 5.74−5.80 (1H, m, CH=), 7.30−7.42 (3H, m, ArH), 7.60−7.76 (4H, m, ArH). *m/z* (ISMS): 370.5 (MH^+). Found (FAB-HRMS): 370.2016. Calcd for $C_{22}H_{28}O_4N$ (MH^+): 370.2018.

***tert*-Butyl 4(*R,S*)-Acetoxy-5(*S*)-[(*tert*-butoxy)carbonylamino]-6-(2-naphthyl)hex-2-enoate, 22.** To a solution of acetate **21** (5.7 g, 15.4 mmol) in CH_2Cl_2 (40 mL) was bubbled O_3 gas at −78 °C until a blue color persisted. To the above solution, was added Me_2S (11 mL, 154 mmol), and the mixture was stirred for 30 min. The mixture was dried over $MgSO_4$. Concentration under reduced pressure gave an oily residue of a crude aldehyde, which was used immediately in the next step without further purification. To a stirred suspension of LiCl (1.57 g, 37 mmol) in MeCN (10 mL) under argon were added $(EtO)_2P(O)CH_2CO_2{}^tBu$ (8.7 mL, 37 mmol) and DIPEA (6.4 mL, 37 mmol) at 0 °C. After 20 min, the above aldehyde in MeCN (20 mL) was added to the above mixture at 0 °C, and the mixture was stirred at this temperature for 8 h. The mixture was concentrated under reduced pressure, and the residue was extracted with EtOAc. The extract was washed successively with saturated aqueous citric acid and H_2O and dried over $MgSO_4$. Concentration under reduced pressure followed by chromatography over silica gel with EtOAc/*n*-hexane (1:2) gave enoates **22** (2.1 g, 29% yield from **21**) as a white amorphous semisolid.

Found: C, 68.97; H, 7.60; N, 2.92. $C_{27}H_{35}O_6N$ Calcd: C, 69.06; H, 7.51; N, 2.98. ^{1}H NMR (270 MHz, $CDCl_3$) δ: 1.34−1.38 (9H, br, *tert*-Bu), 1.43−1.47 (9H, br, *tert*-Bu), 2.13−2.17 (3H, br, Me), 2.91−2.99 (2H, br, CH_2), 4.22−4.32 (1H, br, 5-H), 4.71−4.77 (1H, br, 4-H), 5.42−5.46 (1H, br, NH), 5.79−5.99 (1H, m, CH=), 6.70−6.83 (1H, m, CH=), 7.43−7.49 (3H, m, ArH), 7.77−7.82 (4H, m, Ar). *m/z* (FAB-LRMS): 468 [$(M-H)^-$], 305, 199, 153, 151, and 46 (base peak). Found (FAB-HRMS): 468.2375. Calcd for $C_{27}H_{34}O_6N$ [$(M-H)^-$]: 468.2386.

***tert*-Butyl 5(*S*)-[(*tert*-Butoxy)carbonylamino]-6-(2-naphthyl)hex-3-enoate (Boc-L-Nal=Gly-O^{t}Bu), 23.** To a stirred slurry of Sm (900 mg, 6.0 mmol) in dry THF (20 mL) under argon at room temperature was added a solution of CH_2I_2 (322 μL, 4.0 mmol) in dry THF (20 mL), and the slurry was stirred at room temperature for 2 h until a dark green color persisted. To a stirred solution of enoate **22** (600 mg, 1.3 mmol) in dry THF (16 mL) in the other vessel were added *tert*-BuOH (8 mL, excess) and the above SmI_2 solution (38 mL, 3.8 mmol) under argon at room temperature, and the mixture was stirred for 1 h. The reaction was then quenched with saturated aqueous NH_4Cl (10 mL) at 4 °C, and the mixture was extracted with Et_2O (20 mL). The extract was washed with saturated aqueous NH_4Cl and brine and dried over $MgSO_4$. Concentration under reduced pressure followed by chromatography over silica gel with EtOAc/*n*-hexane (1:4) gave the enoate **23** (530 mg, 95% yield from **22**) as white crystals.

Mp: 80−82 °C (from *n*-hexane). Found: C, 73.17; H, 8.17; N, 3.39. $C_{25}H_{33}O_4N$ Calcd: C, 72.96; H, 8.08; N, 3.40. $[\alpha]^{25}_D$ 11.00 (*c* 1.09, $CHCl_3$). ^{1}H NMR (400 MHz, $CDCl_3$) δ: 1.37 (9H, s, *tert*-Bu), 1.41 (9H, s, *tert*-Bu), 2.93 (2H, d, *J* = 6.4 Hz, 6-CH_2), 2.98 (2H, d, *J* = 6.8 Hz, 2-CH_2), 4.48−4.59 (1H, br, NH), 5.43 (1H, t, *J* = 11.2 Hz, 5-H), 5.55 (1H, dd, *J* = 15.6, 5.6 Hz, CH=), 5.61−5.69 (1H, br, CH=), 7.31−7.46 (3H, m, ArH), 7.60−7.62 (1H, br, ArH), 7.74−7.78 (3H, m, ArH). *m/z* (ISMS): 412.0 (MH^+). Found (FAB-HRMS): 412.2491. Calcd for $C_{25}H_{34}O_4N$ (MH^+): 412.5418.

5(*S*)-[(Fluoren-9-ylmethoxy)carbonylamino]-6-(2-naphthyl)hex-3-enoic Acid (Fmoc-L-Nal=Gly-OH), 24. The enoate **23** (1.79 g, 4.35 mmol) was dissolved in TFA (30 mL), anisole (472 μL, 4.35 mmol) was added to the solution at 4 °C, and the mixture was stirred at room temperature for 2 h. The mixture was concentrated under reduced pressure and dissolved in THF and H_2O (1:1 (v/v) 20 mL). To the stirred solution were added Fmoc-OSu (1.47 g, 4.35 mmol) and Et_3N (10 mL, 71.7 mmol) at 4 °C, and the mixture was stirred at room temperature for 8 h. The mixture was acidified with aqueous 1 M HCl and was extracted with EtOAc. The extract was washed with aqueous 0.1 M HCl and brine and dried over $MgSO_4$. Concentration under reduced pressure followed by chromatography over silica gel with EtOAc/*n*-hexane (3:1) gave the enoic acid **24** (1.61 g, 78% yield from **23**) as white crystals.

Mp: 134−136 °C (from *n*-hexane). $[\alpha]^{23}_D$ −2.75 (*c* 0.73, $CHCl_3$). ^{1}H NMR (400 MHz, $CDCl_3$) δ: 2.96 (2H, br, 6-CH_2), 3.03 (2H, br, 2-CH_2), 4.14 (1H, t, *J* = 6.6 Hz, ArH), 4.32 (1H, dd, *J* = 14.9, 7.2 Hz, CH=), 4.38 (1H, m, CH=) 4.54 (1H, d, *J* = 7.6 Hz, CH_2), 4.81 (1H, br, 5-H), 5.62 (1H, br, NH), 7.18−7.28 (2H, m, ArH), 7.30−7.52 (5H, m, ArH), 7.57−7.63 (2H, m, ArH), 7.70−7.79 (6H, m, ArH). *m/z* (ISMS): 478.0 (MH^+). Found (FAB-HRMS): 478.2016. Calcd for $C_{31}H_{28}O_4N$ (MH^+): 478.2018.

H-D-Tyr(O^{t}Bu)-Arg(Pbf)-Arg(Pbf)-Nal-ψ[(*E*)-CH=CH]-Gly-NHNHCO−Wang Resin. On the hydrazide resin, were coupled successively Fmoc-D-Tyr(O^{t}Bu)-OH, Fmoc-Nal-ψ[(*E*)-CH=CH]-Gly-OH, and Fmoc-Arg(Pbf)-OH by use of the procedure identical with that described for the preparation of H-D-Tyr(O^{t}Bu)-Arg(Pbf)-Arg(Mts)-ψ[(*E*)-CH=CH]-Nal-Gly-NHNHCO−Wang resin to afford the protected **37c** resin.

***cyclo*(-D-Tyr-Arg-Arg-Nal-ψ[(*E*)-CH=CH]-Gly-)·2TFA (37c).** By use of a procedure identical with that described for the preparation of **37a**, the protected **37c** resin (173 mg, 0.13 mmol) was converted into 7.0 mg (7.4 μmol, 5.9%) of the title compound **37c**, as a freeze-dried powder.

$[\alpha]^{21}_D$ −43.1 (*c* 0.33, H_2O). t_R = 24.3 min (linear gradient of MeCN in H_2O, 10 to 40% over 30 min). *m/z* (ISMS): 713.0

(MH$^+$). Found (FAB-HRMS): 713.3911. Calcd for $C_{37}H_{49}O_5N_{10}$ (MH$^+$): 713.3887.

***tert*-Butyl 2(*S*)-[[2(*S*)-[(*tert*-butoxy)carbonyamino]-5-[[imino[[(2,4,6-trimethylphenyl)sulfonyl]amino]methyl]-amino]pentyl]amino]-3-(2-naphthyl) Propanoate [Boc-L-Arg(Mts)-ψ[CH$_2$–NH]-L-Nal-O^{t}Bu], 26.** To a stirred solution of **25** (5.0 g, 10 mmol) in toluene/CH_2Cl_2 (1:1 (v/v), 50 mL) was added dropwise a solution of DIBAL-H in toluene (1.0 M, 60 mL, 60 mmol) at −50 °C under argon, and the mixture was stirred for 4 h at −78 °C. The reaction was quenched with saturated aqueous citric acid at −78 °C, and the organic solvents were concentrated under reduced pressure. The residue was extracted with EtOAc, and the extract was washed successively with saturated aqueous citric acid and brine and dried over $MgSO_4$. Concentration under reduced pressure gave a crude aldehyde (Boc-Arg(Mts)-H), which was used in the following step without further purification. To the stirred solution of Boc-Arg(Mts)-H in $ClCH_2CH_2Cl$/DMF (1:6 (v/v), 100 mL), were added H-L-Nal-O^{t}Bu (5.4 g, 20 mmol) and AcOH (1.1 mL, 20 mmol) at 4 °C and stirred for 10 min. $NaBH(OAc)_3$ (6.4 g, 30 mmol) was added to the above mixture at 4 °C and stirred for 8 h with warming to room temperature. The mixture was concentrated under reduced pressure, and the residue was extracted with $CHCl_3$. The extract was washed with aqueous 5% $NaHCO_3$ and brine and dried over $MgSO_4$. Concentration under reduced pressure gave an oily residue, which was purified by chromatography over silica gel with $CHCl_3$/MeOH (39:1) to yield 3.4 g (4.9 mmol, 49% yield from **25**) of compound **26** as a yellow oil.

$[\alpha]^{23}_D$ 4.08 (*c* 1.96, $CHCl_3$). ^{1}H NMR (270 MHz, $CDCl_3$) δ: 1.24 (9H, s, *tert*-Bu), 1.32 (9H, s, *tert*-Bu), 1.55 (2H, br m, 4-CH$_2$), 1.74 (2H, br m, 3-CH$_2$), 2.25 (3H, s, Ar-*p*-Me), 2.67 (6H, s, Ar-*o*-Me), 3.08 (2H, br m, 5-CH$_2$), 3.20 (2H, br, 3-CH$_2$), 3.34 (2H, br, 1-CH$_2$), 3.62 (1H, br, 2-H), 3.82 (1H, br, 2-H), 3.99 (1H, br, NH), 5.95 (1H, br, NH), 6.61 (3H, br, guanidino), 6.87 (2H, s, Ar-*m*-H), 7.36–7.44 (3H, m, ArH), 7.67–7.75 (4H, m, ArH). *m/z* (ISMS): 697.0 (MH$^+$). Found (FAB-HRMS): 696.3812. Calcd for $C_{37}H_{54}O_6N_5S$ (MH$^+$): 696.3795.

***tert*-Butyl 2(*S*)-[*N*-[2(*S*)-[(*tert*-Butoxy)carbonylamino]-5-[[imino[[(2,4,6-trimethylphenyl)sulfonyl]amino]methyl]-amino]pentyl](phenylmethoxy)carbonylamino]-3-(2-naphthyl)propanoate [Boc-Arg(Mts)-ψ[CH$_2$–N(Cbz)]-Nal-O^{t}Bu], 27.** To a stirred solution of propanoate **26** (1.4 g, 2.0 mmol) in DMF (100 mL) at 4 °C, were added Cbz-Cl (0.69 g, 4.0 mmol) and Et_3N (560 μL, 4.0 mmol) and stirred at room temperature for 8 h. The mixture was concentrated under reduced pressure and extracted with EtOAc. The extract was washed with saturated aqueous citric acid, saturated aqueous $NaHCO_3$, and brine and dried over $MgSO_4$. Concentration under reduced pressure followed by chromatography over silica gel with EtOAc/*n*-hexane (1:1) gave the title compound **27** (1.6 g, 77% yield from **26**) as a yellow oil.

$[\alpha]^{23}_D$ −36.44 (*c* 0.67, $CHCl_3$). ^{1}H NMR (270 MHz, $CDCl_3$) δ: 1.39 (9H, s, *tert*-Bu), 1.42 (9H, s, *tert*-Bu), 1.47 (2H, s, 4-CH$_2$), 1.64 (2H, br, 3-CH$_2$), 2.42 (3H, s, Ar-*p*-Me), 2.65 (6H, s, Ar-*o*-Me), 2.98 (2H, br, 5-CH$_2$), 3.27 (2H, br, 3-CH$_2$), 3.31 (2H, br, 1-CH$_2$), 3.40 (1H, br, 2-H), 4.24 (1H, br, 2-H), 5.08 (2H, s, CH$_2$), 5.90 (1H, br, NH), 6.13 (3H, br, guanidino), 6.86 (2H, s, Ar-*m*-H), 7.26 (5H, s, ArH), 7.31–7.46 (3H, m, ArH), 7.54–7.75 (4H, m, ArH). *m/z* (ISMS): 831.5 (MH$^+$). Found (FAB-HRMS): 830.4153. Calcd for $C_{45}H_{60}O_6N_5S$ (MH$^+$): 830.4163.

2(*S*)-[*N*-[2(*S*)-[(Fluoren-9-ylmethoxy)carbonylamino]-5-[[imino[[(2,4,6-trimethylphenyl)sulfonyl]amino]methyl]-amino]pentyl](phenylmethoxy)carbonylamino]-3-(2-naphthyl)propanoic Acid [Fmoc-Arg(Mts)-ψ[CH$_2$–N(Cbz)]-Nal-OH], 28. The propanoate **27** (1.3 g, 1.57 mmol) was dissolved in TFA (30 mL), anisole (170 μL, 1.57 mmol) was added to the solution at 4 °C, and the mixture was stirred at room temperature for 2 h. The mixture was concentrated under reduced pressure and dissolved in THF and H_2O (1:1 (v/v) 100 mL). To the stirred solution were added Fmoc-OSu (530 mg, 1.57 mmol) and Et_3N (10 mL, 71.7 mmol) at 4 °C, and the mixture was stirred at room temperature for 8 h. The mixture was acidified with aqueous 1 M HCl and extracted with EtOAc. The extract was washed with aqueous 0.1 M HCl and brine and dried over $MgSO_4$. Concentration under reduced pressure followed by chromatography over silica gel with EtOAc/*n*-hexane (4:1) gave the propanoic acid **28** (1.39 g, 99% yield from **27**) as white crystals.

Mp: 156–158 °C (from *n*-hexane). $[\alpha]^{24}_D$ −8.17 (*c* 1.96, $CHCl_3$). ^{1}H NMR (270 MHz, $CDCl_3$) δ: 1.85 (2H, br, 4-CH$_2$), 1.93 (2H, br, 3-CH$_2$), 2.11 (3H, s, Ar-*p*-Me), 2.47 (6H, s, Ar-*o*-Me), 3.03 (2H, br, 5-CH$_2$), 3.22 (2H, br, 3-H), 3.37 (2H, br, 1-CH$_2$), 4.08 (1H, br, ArH), 4.15 (2H, br, CH$_2$), 4.30 (1H, br, 2-H), 5.16 (1H, br, NH), 6.36 (3H, br, guanidino), 6.83 (2H, s, Ar-*m*-H) 7.25 (5H, s, ArH), 7.29–7.40 (6H, m, ArH), 7.50–7.83 (9H, m, ArH). *m/z* (ISMS): 897.0 (MH$^+$). Found (FAB-HRMS): 896.3693. Calcd for $C_{51}H_{54}O_8N_5S$ (MH$^+$): 896.3710.

H-D-Tyr(O^{t}Bu)-Arg(Pbf)-Arg(Mts)-ψ[CH$_2$–NH]-Nal-Gly-NHNHCO–Wang Resin. On the hydrazide resin were coupled successively Fmoc-Gly-OH, Fmoc-Arg-ψ[CH$_2$–N(Cbz)]-Nal-OH, Fmoc-Arg(Pbf)-OH, and Fmoc-D-Tyr(O^{t}Bu)-OH by use of a procedure identical with that described for the preparation of H-D-Tyr(O^{t}Bu)-Arg(Pbf)-Arg(Mts)-ψ[(*E*)-CH=CH]-Nal-Gly-NHNHCO–Wang resin to afford the protected **37b** resin.

***cyclo*(-D-Tyr-Arg-Arg-ψ[CH$_2$–NH]-Nal-Gly-)·3TFA (37b).** By use of a procedure identical with that described for the preparation of **37a**, the protected **37b** (200 mg, 0.15 mmol) was converted into 0.6 mg (0.57 μmol, 0.86%) of the title compound **37b**, as a freeze-dried powder.

$[\alpha]^{21}_D$ −22.6 (*c* 0.27, H_2O). t_R = 19.3 min (linear gradient of MeCN in H_2O, 10 to 40% over 30 min). *m/z* (ISMS): 717.0 (MH$^+$). Found (FAB-HRMS): 716.4016. Calcd for $C_{36}H_{49}O_5N_{11}$ (MH$^+$): 716.3996.

***tert*-Butyl 2(*S*)-[[2-[(*tert*-Butoxy)carbonylamino]-3-(2-naphthyl)propyl]amino]acetate [Boc-L-Nal-ψ[CH$_2$–NH]-Gly-O^{t}Bu], 30.** To a stirred solution of Boc-Nal-NMe(OMe) **29** (5.5 g, 15 mmol) in toluene/CH_2Cl_2 (1:1 (v/v) 50 mL) was added dropwise a solution of DIBAL-H in toluene (1.0 M, 62 mL, 62 mmol) at −78 °C under argon, and the mixture was stirred at −78 °C for 4 h. The reaction was quenched with saturated aqueous citric acid at −78 °C, and organic solvents were concentrated under reduced pressure. The residue was extracted with EtOAc, and the extract was washed successively with saturated aqueous citric acid and brine and dried over $MgSO_4$. Concentration under reduced pressure gave a crude aldehyde (Boc-Nal-H), which was used in the following step without further purification. To the stirred solution of Boc-Nal-H in $ClCH_2CH_2Cl$/DMF (1:6 (v/v), 200 mL), was added H-Gly-O^{t}Bu·AcOH (5.8 g, 31 mmol) at 4 °C and stirred for 10 min. $NaBH(OAc)_3$ (9.8 g, 46 mmol) was added to the above mixture at 4 °C and stirred for 8 h with warming to room temperature. The mixture was concentrated under reduced pressure, and the residue was extracted with $CHCl_3$. The extract was washed with aqueous 5% $NaHCO_3$ and brine and dried over $MgSO_4$. Concentration under reduced pressure gave an oily residue, which was purified by chromatography over silica gel with $CHCl_3$ to yield 3.2 g (7.7 mmol, 50% yield from **29**) of compound **30** as a yellow oil.

$[\alpha]^{22}_D$ −0.67 (*c* 4.47, $CHCl_3$). ^{1}H NMR (400 MHz, $CDCl_3$) δ: 1.38 (9H, s, *tert*-Bu), 1.47 (9H, s, *tert*-Bu), 2.87 (2H, br, CH$_2$), 3.02 (2H, br, 3-CH$_2$), 3.85–3.94 (2H, m, 1-CH$_2$), 4.09–4.21 (1H, m, 2-H), 5.44 (1H, br, NH), 6.45 (1H, br, NH), 7.29–7.36 (2H, m, Ar–H), 7.41–7.48 (2H, m, ArH), 7.60–7.62 (1H, m, ArH), 7.72–7.83 (2H, m, ArH). *m/z* (ISMS): 415.5 (MH$^+$). Found (FAB-HRMS): 415.2594. Calcd for $C_{24}H_{35}O_4N_2$ (MH$^+$): 415.2597.

***tert*-Butyl 2(*S*)-[*N*-[2-[(*tert*-Butoxy)carbonylamino]-3-(2-naphthyl)propyl](phenylmethoxy)carbonylamino]acetate [Boc-L-Nal-ψ[CH$_2$–N(Cbz)]-Gly-O^{t}Bu], 31.** To a stirred solution of acetate **30** (5.0 g, 12.1 mmol) in DMF (100 mL) at 4 °C were added Cbz-Cl (20.6 g, 121 mmol) and DIPEA (21.7 mL, 121 mmol), and the mixture was stirred at room temperature for 8 h. The mixture was concentrated under reduced pressure and extracted with EtOAc. The solution was washed with saturated aqueous citric acid, saturated aqueous $NaHCO_3$, and brine and dried over $MgSO_4$. Concentration under

reduced pressure followed by chromatography over silica gel with EtOAc/*n*-hexane (1:2) gave the title compound **31** (4.0 g, 60% yield from **30**) as white crystals.

Mp: 107−109 °C (from *n*-hexane). Found: C, 70.01; H, 7.42 N, 4.98. Calcd for $C_{32}H_{40}O_6N_2$: C, 70.05; H, 7.35; N, 5.11. $[\alpha]^{23}_D$ −14.73 (*c* 0.48, $CHCl_3$). ^{1}H NMR (400 MHz, $CDCl_3$) δ: 1.34 (9H, s, *tert*-Bu), 1.35 (9H, s, *tert*-Bu), 2.94 (2H, br, CH_2), 3.37 (2H, br, 3-CH_2), 3.88 (2H, m, 1-CH_2), 4.05 (1H, m, 2-H), 4.94 (1H, br, NH), 5.13 (2H, s, CH_2), 7.28−7.33 (5H, br, ArH), 7.35−7.47 (3H, m, ArH), 7.74−7.81 (4H, m, ArH). *m/z* (ISMS): 549.5 (MH^+). Found (FAB-HRMS): 549.2953. Calcd for $C_{32}H_{41}O_6N_2$ (MH^+): 549.2965.

2(*S*)-[*N*-[2-[(Fluoren-9-ylmethoxy)carbonylamino]-3-(2-naphthyl)propyl](phenylmethoxy)carbonylamino]-acetic Acid [Fmoc-L-Nal-ψ[CH_2−N(Cbz)]-Gly-OH], 32. The acetate **31** (4.0 g, 7.29 mmol) was dissolved in TFA (30 mL), anisole (792 μL, 7.29 mmol) was added to the solution at 4 °C, and the mixture was stirred at room temperature for 2 h. The mixture was concentrated under reduced pressure and dissolved in THF and H_2O (1:1 (v/v) 100 mL). To the stirred solution, were added Fmoc-OSu (2.46 g, 7.29 mmol) and Et_3N (10 mL, 71.7 mmol) at 4 °C, and the mixture was stirred at room temperature for 8 h. The mixture was acidified with aqueous 1 M HCl and was extracted with EtOAc. The extract was washed with aqueous 0.1 M HCl and brine and dried over $MgSO_4$. Concentration under reduced pressure followed by chromatography over silica gel with $CHCl_3$/MeOH (39:1) gave the title compound **32** (4.20 g, 94% yield from **31**) as a yellow oil.

$[\alpha]^{23}_D$ −5.01 (*c* 4.79, $CHCl_3$). ^{1}H NMR (400 MHz, $CDCl_3$) δ: 2.99 (2H, d, J = 6.4 Hz, 3-CH_2), 3.41 (2H, s, CH_2), 4.00 (2H, br, 1-CH_2), 4.08 (1H, t, J = 6.6 Hz, Ar−H), 4.24 (1H, t, J = 6.2 Hz, 2-H), 4.27 (2H, br, CH_2), 5.05 (2H, s, CH_2), 5.53 (1H, d, J = 8.0 Hz, NH), 7.18 (5H, s, Ar−H) 7.30−7.50 (8H, m, ArH), 7.61−7.73 (7H, m, ArH). *m/z* (ISMS): 615.0 (MH^+). Found (FAB-HRMS): 615.2509. Calcd for $C_{38}H_{35}O_6N_2$ (MH^+): 615.2495.

H-D-Tyr(O^{t}Bu)-Arg(Pbf)-Arg(Pbf)-Nal-ψ[CH_2−N(Cbz)]-Gly-NHNHCO−Wang Resin. On the hydrazide resin, were coupled successively Fmoc-D-Tyr(O^{t}Bu)-OH, Fmoc-Nal-ψ[CH_2−N(Cbz)]-Gly-OH, and Fmoc-Arg(Pbf)-OH by use of a procedure identical with that described for the preparation of H-D-Tyr-(O^{t}Bu)-Arg(Pbf)-Arg(Mts)-ψ[(*E*)-CH=CH]-Nal-Gly-NHNHCO−Wang resin to afford the protected **37d** resin.

***cyclo*(-D-Tyr-Arg-Arg-Nal-ψ[CH_2−NH]-Gly-)·3TFA (37d).** By use of a procedure identical with that described for the preparation of **37a**, the protected **37d** (173 mg, 0.13 mmol) was converted into 7.0 mg (7.4 μmol, 5.9%) of the title compound **37d**, as a freeze-dried powder.

$[\alpha]^{19}_D$ −58.0 (*c* 0.69, H_2O). t_R = 21.0 min (linear gradient of MeCN in H_2O, 10 to 40% over 30 min). *m/z* (ISMS): 717.0 (MH^+). Found (FAB-HRMS): 716.4003. Calcd for $C_{36}H_{49}O_5N_{11}$ (MH^+): 716.3996.

Cell Culture. Human T-cell lines, MT-4, and MOLT-4 cells were grown in RPMI 1640 medium containing 10% heat-inactivated fetal calf serum, 100 IU/mL penicillin, and 100 μg/mL streptomycin.

Virus. A strain of X4-HIV-1, HIV-1$_{IIIB}$, was used for the anti-HIV assay. This virus was obtained from the culture supernatant of HIV-1 persistently infected MOLT-4/HIV-1$_{IIIB}$ cells and stored at −80 °C until used.

Anti-HIV-1 Assay. Anti-HIV-1 activity was determined based on the protection against HIV-1-induced cytopathogenicity in MT-4 cells. Various concentrations of test compounds were added to HIV-1-infected MT-4 cells at a multiplicity of infection (MOI) of 0.01 and placed in wells of a flat-bottomed microtiter tray (1.5 × 10^4 cells/well). After 5 days incubation at 37 °C in a CO_2 incubator, the number of viable cells was determined using the 3-(4,5-dimethylthiazol-2-yl)-2,5-diphenyltetrazolium bromide (MTT) method (EC_{50}).[48] Cytotoxicity of compounds was determined based on the viability of mock-infected cells using the MTT method (CC_{50}). 3′-Azido-3′-dideoxythymidine (AZT) was tested as a control.

[^{125}I]-SDF-1 Binding and Displacement. Stable CHO cell transfectants expressing CXCR4 variants were prepared as described previously.[49] CHO transfectants were harvested by treatment with trypsin/EDTA, allowed to recover in complete growth medium (MEM-α, 100 μg/mL penicillin, 100 μg/mL streptomycin, 0.25 μg/mL amphotericin B, 10% (v/v)) for 4−5 h, and then washed in cold binding buffer (PBS containing 2 mg/mL BSA). For ligand binding, the cells were resuspended in binding buffer at 1 × 10^7 cells/mL, and 100 μL aliquots were incubated with 0.1 nM of [^{125}I]-SDF-1 (PerkinElmer Life Sciences) for 2 h on ice under constant agitation. Free and bound radioactivities were separated by centrifugation of the cells through an oil cushion, and bound radioactivity was measured with a gamma counter (Cobra, Packard, Downers Grove, IL). Inhibitory activity of FC131 analogues was determined based on the inhibition of [^{125}I]-SDF-1-binding to CXCR4 transfectants (IC_{50}).

NMR Spectroscopy (37a and 37c). The peptide sample was dissolved in DMSO-d_6 at a concentration of 5 mM. ^{1}H NMR spectra of the peptides were recorded at 300 K. The assignments of the proton resonances were achieved by use of ^{1}H−^{1}H COSY spectra. $^3J(H^N, H^\alpha)$ coupling constants were measured from one-dimensional spectra. The mixing time for the nuclear Overhauser spectroscopy (NOESY) experiments was set at 400 ms. NOESY spectra were composed of 512 real points in the F2 dimension and 256 real points, which were zero-filled to 256 points in the F1 dimension, with 144 scans per t1 increment. The cross-peak intensities were evaluated by relative buildup rates of the cross peaks. Temperature dependence of the chemical shifts of all of the amide bonds was investigated in **37a** and **37c**. The only temperature coefficient for the NH of Arg^5 was small, but NOE was not observed between the D-Tyr^3 C$^\alpha$H and the Arg^5 NH in both **37a** and **37c**. Thus, no hydrogen bond restraints were used in the simulated annealing calculations.

Calculation of Structures. The structure calculations were performed on a Silicon Graphics Origin 2000 workstation with the NMR refine program within the Insight II/Discover package using the consistent valence force field (CVFF).[61] Pseudoatoms were defined for the methylene protons of Nal^1, D-Tyr^3, Arg^4, and Arg^5, prochiralities of which were not identified by ^{1}H NMR data. The restraints, in which the Gly^2 α-methylene participated, were defined for the separate protons without definition of the prochiralities. The dihedral ϕ angle constraints were calculated based on the Karplus equation: $^3J(H^N,H^\alpha) = 6.7\cos^2(\theta - 60°) - 1.3\cos(\theta - 60°) + 1.5$.[52] Lower and upper angle errors were set to 15°. The NOESY spectrum with a mixing time of 400 ms was used for the estimation of the distance restraints between protons. The NOE intensities were classified into three categories (strong, medium, and weak) based on the number of contour lines in the cross peaks to define the upper-limit distance restraints (2.7, 3.5, and 5.0 Å, respectively). The upper-limit restraints were increased by 1.0 Å for the involved pseudoatoms. Lower bounds between nonbonded atoms were set to their van der Waals radii (1.8 Å). These distance and dihedral angle restraints were included with force constants of 25−100 kcal/mol·Å^2 and 25−100 kcal/mol·rad^2, respectively. The 50 initial structures generated by the NMR refine program randomly were subjected to the simulated annealing calculations. The final minimization stage was achieved until the maximum derivative became less than 0.01 kcal/mol·Å^2 by the steepest descents and conjugate gradients methods.

Acknowledgment. This work was supported in part by a 21st Century COE Program "Knowledge Information Infrastructure for Genome Science", a Grant-in-Aid for Scientific Research from the Ministry of Education, Culture, Sports, Science and Technology, Japan and the Japan Health Science Foundation. Computation time was provided by the Supercomputer Laboratory, Institute for Chemical Research, Kyoto University. S.U. is

grateful for a Research Fellowship from the Japan Society for the Promotion of Science for Young Scientists.

Supporting Information Available: HPLC charts for synthetic compounds of **37a**, **37b**, **37c**, **37d**, and **37f**. These materials are available free of charge via the Internet at http://pubs.acs.org.

References

(1) Kaltenbronn, J. S.; Hudspeth, J. P.; Lunney, E. A.; Michniewicz, B. M.; Nicolaides, E. D.; Repine, J. T.; Roark, W. H.; Stier, M. A.; Tinney, F. J.; Woo, P. K. W.; Essenburg, A. D. Renin inhibitors containing isosteric replacements of the amide bond connecting the P_3 and P_2 sites. *J. Med. Chem.* **1990**, *33*, 838–845.

(2) Ibuka, T.; Habashita, H.; Otaka, A.; Fujii, N. A highly stereoselective synthesis of (*E*)-alkene dipeptide isosteres via organocyanocopper–lewis acid mediated reaction. *J. Org. Chem.* **1991**, *56*, 4370–4382.

(3) Wipf, P.; Fritch, P. C. S_N2' reactions of peptide aziridines. A cuprate-based approach to (*E*)-alkene isosteres. *J. Org. Chem.* **1994**, *59*, 4875–4886.

(4) Fujii, N.; Nakai, K.; Tamamura, H.; Otaka, A.; Mimura, N.; Miwa, Y.; Taga, T.; Yamamoto, Y.; Ibuka, T. S_N2' ring opening of aziridines bearing an α,β-unsaturated ester group with organocopper reagents. A new stereoselective synthetic route to (*E*)-alkene dipeptide isosteres. *J. Chem. Soc., Perkin Trans. 1* **1995**, 1359–1371.

(5) Daly, M. J.; Ward, R. A.; Thompson, D. F.; Procter, G. Allylsilanes in organic synthesis; stereoselective synthesis of *trans*-alkene peptide isosteres. *Tetrahedron Lett.* **1995**, *36*, 7545–7548.

(6) Tamamura, H.; Hiramatsu, K.; Miyamoto, K.; Omagari, A.; Oishi, S.; Nakashima, H.; Yamamoto, N.; Kuroda, Y.; Nakagawa, T.; Otaka, A.; Fujii, N. Synthesis and evaluation of pseudopeptide analogues of a specific CXCR4 inhibitor, T140: The insertion of an (*E*)-alkene dipeptide isostere into the βII′-turn moiety. *Bioorg. Med. Chem. Lett.* **2002**, *12*, 923–928.

(7) Tamamura, H.; Koh, Y.; Ueda, S.; Sasaki, Y.; Yamasaki, T.; Aoki, M.; Maeda, K.; Watai, Y.; Arikuni, H.; Otaka, A.; Mitsuya, H.; Fujii, N. Reduction of peptide character of HIV protease inhibitors that exhibit nanomolar potency against multi-drug resistant HIV-1 strains. *J. Med. Chem.* **2003**, *46*, 1764–1768.

(8) Tamamura, H.; Yamashita, M.; Muramatsu, H.; Ohno, H.; Ibuka, T.; Otaka, A.; Fujii, N. Regiospecific ring-opening reactions of aziridines bearing an α,β-unsaturated ester group with trifluoroacetic acid or methanesulfonic acid: Application to the stereoselective synthesis of (*E*)-alkene dipeptide isosteres. *Chem. Commun.* **1997**, 2327–2328.

(9) Tamamura, H.; Yamashita, M.; Nakajima, Y.; Sakano, K.; Otaka, A.; Ohno, H.; Ibuka, T.; Fujii, N. Regiospecific ring-opening reactions of β-aziridinyl α,β-enoates with acids: application to the stereoselective synthesis of a couple of diastereoisomeric (*E*)-alkene dipeptide isosteres from a single β-aziridinyl α,β-enoate and to the convenient preparation of amino alcohols bearing α,β-unsaturated ester groups. *J. Chem. Soc., Perkin Trans. 1*, **1999**, 2983–2996.

(10) Oishi, S.; Tamamura, H.; Yamashita, M.; Odagaki, Y.; Hamanaka, N.; Otaka, A.; Fujii, N. Stereoselective synthesis of a set of two functionalized (*E*)-alkene dipeptide isosteres of L-amino acid-L-Glu and L-amino acid-D-Glu. *J. Chem. Soc., Perkin Trans. 1* **2001**, 2445–2451.

(11) Nakamura, E.; Aoki, S.; Sekiya, K.; Oshino, H.; Kuwajima, I. Carbon–carbon bond-forming reactions of zinc homoenolate of esters. A novel three-carbon nucleophile with general synthetic utility. *J. Am. Chem. Soc.* **1987**, *109*, 8056–8066.

(12) Ochiai, H.; Tamaru, Y.; Tsubaki, K.; Yoshida, Z. Unsaturated ester synthesis via copper(I)-catalyzed allylation of zinc esters. *J. Org. Chem.* **1987**, *52*, 4418–4420.

(13) Yeh, M. C. P.; Knochel, P. 2-Cyanoethylzinc iodide: A new reagent with reactivity umpolung.*Tetrahedron Lett.* **1988**, *29*, 2395–2396.

(14) Knochel, P.; Yeh, M. C. P.; Berk, S. C.; Talbert, J. Synthesis and reactivity toward acyl chlorides and enones of the new highly functionalized copper reagents RCu(CN)ZnI. *J. Org. Chem.* **1988**, *53*, 2390–2392.

(15) Zhu, L.; Wehmeyer, R. M.; Rieke, R. D. The direct formation of functionalized alkyl(aryl)zinc halides by oxidative addition of highly reactive zinc with organic halides and their reactions with acid chlorides, α,β-unsaturated ketones, and allylic, aryl, and vinyl halides. *J. Org. Chem.* **1991**, *56*, 1445–1453.

(16) Fujii, N.; Oishi, S.; Hiramatsu, K.; Araki, T.; Ueda, S.; Tamamura, H.; Otaka, A.; Kusano, S.; Terakubo, S.; Nakashima, H.; Broach, J. A.; Trent, J. O.; Wang, Z.; Peiper, S. C. Molecular-size reduction of a potent CXCR4–chemokine antagonist using orthogonal combination of conformation- and sequence-based libraries. *Angew. Chem., Int. Ed.* **2003**, *42*, 3251–3253.

(17) Koshiba, T.; Hosotani, R.; Miyamoto, Y.; Ida, J.; Tsuji, S.; Nakajima, S.; Kawaguchi, M.; Kobayashi, H.; Doi, R.; Hori, T.; Fujii, N.; Imamura, M. Expression of stromal cell-derived factor 1 and CXCR4 ligand receptor system in pancreatic cancer: a possible role for tumor progression. *Clin. Cancer. Res.* **2000**, *6*, 3530–3535.

(18) Müller, A.; Homey, B.; Soto, H.; Ge, N.; Catron, D.; Buchanan, M. E.; McClanahan, T.; Murphy, E.; Yuan, W.; Wagner, S. N.; Barrera, J. L.; Mohar, A.; Verastegui, E.; Zlotnik, A. Involvement of chemokine receptors in breast cancer metastasis. *Nature* **2001**, *410*, 50–56.

(19) Tamamura, H.; Hori, A.; Kanzaki, N.; Hiramatsu, K.; Mizumoto, M.; Nakashima, H.; Yamamoto, N.; Otaka, A.; Fujii, N. T140 analogs as CXCR4 antagonists identified as anti-metastatic agents in the treatment of breast cancer. *FEBS Lett.* **2003**, *550*, 79–83.

(20) Feng, Y.; Broder, C. C.; Kennedy, P. E.; Berger, E. A. HIV-1 entry co-factor: Functional cDNA cloning of a seven-transmembrane, G protein-coupled receptor. *Science* **1996**, *272*, 872–877.

(21) Nanki, T.; Hayashida, K.; EI–Gabalawy, H. S.; Suson, S.; Shi, K.; Girschick, H. J.; Yavuz, S.; Lipsky, P. E. Stromal cell-derived factor-1-CXC chemokine receptor interactions play a central role in CD4$^+$ T cell accumulation in rheumatoid arthritis synovium. *J. Immunol.* **2000**, *165*, 6590–6598.

(22) Tamamura, H.; Fujisawa, M.; Hiramatsu, K.; Mizumoto, M.; Nakashima, H.; Yamamoto, N.; Otaka, A.; Fujii, N. Identification of a CXCR4 antagonist, a T140 analog, as an anti-rheumatoid arthritis agent. *FEBS Lett.* **2004**, *569*, 99–104.

(23) Murakami, T.; Nakajima, T.; Koyanagi, Y.; Tachibana, K.; Fujii, N.; Tamamura, H.; Yoshida, N.; Waki, M.; Matsumoto, A.; Yoshie, O.; Kishimoto, T.; Yamamoto, N.; Nagasawa, T. A small molecule CXCR4 inhibitor that blocks T cell line-tropic HIV-1 infection. *J. Exp. Med.*, **1997**, *186*, 1389–1393.

(24) Schols, D.; Struyf, S.; Van Damme, J.; Este, J. A.; Henson, G.; De Clercq, E. Inhibition of T-tropic HIV strains by selective antagonization of the chemokine receptor CXCR4. *J. Exp. Med.* **1997**, *186*, 1383–1388.

(25) Donzella, G. A.; Schols, D.; Lin, S. W.; Este J. A.; Nagashima, K. A.; Maddon, P. J.; Allaway, G. P.; Sakmar, T. P.; Henson, G.; De Clercq, E.; Moore, J. P. AMD3100, a small molecule inhibitor of HIV-1 entry via the CXCR4 co-receptor. *Nat. Med.* **1998**, *4*, 72–77.

(26) Doranz, B. J.; Grovit-Ferbas, K.; Sharron, M. P.; Mao, S.-H.; Bidwell Goetz, M.; Daar, E. S.; Doms, R. W.; O'Brien, W. A. A small-molecule inhibitor directed against the chemokine receptor CXCR4 prevents its use as an HIV-1 coreceptor. *J. Exp. Med.* **1997**, *186*, 1395–1400.

(27) Howard, O. M. Z.; Oppenheim, J. J.; Hollingshead, M. G.; Covey, J. M.; Bigelow, J.; McCormack, J. J.; Buckheit, Jr., R. W.; Clanton, D. J.; Turpin, J. A.; Rice, W. G. Inhibition of in vitro and in vivo HIV replication by a distamycin analogue that interferes with chemokine receptor function: a candidate for chemotherapeutic and microbicidal application. *J. Med. Chem.* **1998**, *41*, 2184–2193.

(28) Tamamura, H.; Xu, Y.; Hattori, T.; Zhang, X.; Arakaki, R.; Kanbara, K.; Omagari, A.; Otaka, A.; Ibuka, T.; Yamamoto, N.; Nakashima, H.; Fujii, N. A low molecular weight inhibitor against the chemokine receptor CXCR4: a strong anti-HIV peptide T140. *Biochem. Biophys. Res. Commun.* **1998**, *253*, 877–882.

(29) Tamamura, H.; Omagari, A.; Oishi, S.; Kanamoto, T.; Yamamoto, N.; Peiper, S. C.; Nakashima, H.; Otaka, A.; Fujii, N. Pharmacophore identification of a specific CXCR4 inhibitor, T140, leads to development of effective anti-HIV agents with very high selectivity indexes. *Bioorg. Med. Chem. Lett.* **2000**, *10*, 2633–2637.

(30) Fujii, N.; Nakashima, H.; Tamamura, H. The therapeutic potential of CXCR4 antagonists in the treatment of HIV. *Expert Opin. Invest. Drugs* **2003**, *12*, 185–195.

(31) Fukami, T.; Nagase, T.; Fujita, K.; Hayama, T.; Niiyama, K.; Mase, T.; Nakajima, S.; Fukuroda, T.; Saeki, T.; Nishikibe, M.; Ihara, M.; Yano, M.; Ishikawa, K. Structure–activity relationships of cyclic pentapeptide endothelin A receptor antagonists. *J. Med. Chem.* **1995**, *38*, 4309–4324.

(32) Haubner, R.; Gratias, R.; Diefenbach, B.; Goodman, S. L.; Jonczyk, A.; Kessler, H. Structural and functional aspects of RGD-containing cyclic pentapeptides as highly potent and selective integrin $\alpha V\beta 3$ antagonists. *J. Am. Chem. Soc.* **1996**, *118*, 7461–7472.

(33) Spatola, A. F.; Crozet, Y.; deWit, D.; Yanagisawa, M. Rediscovering an endothelin antagonist (BQ-123): A self-deconvoluting cyclic pentapeptide library. *J. Med. Chem.* **1996**, *39*, 3842−3846.
(34) Wermuth, J.; Goodman, S. L.; Jonczyk, A.; Kessler, H. Stereoisomerism and biological activity of the selective and superactive αVβ3 integrin inhibitor cyclo(−RGDfV-) and its retro-inverso peptide. *J. Am. Chem. Soc.* **1997**, *119*, 1328−1335.
(35) Haubner, R.; Finsinger, D.; Kessler, H. Stereoisomeric peptide libraries and peptidomimetics for designing selective inhibitors of the αVβ3 integrin for a new cancer therapy. *Angew. Chem., Int. Ed. Engl.* **1997**, *36*, 1374−1389.
(36) Porcelli, M.; Casu, M.; Lai, A.; Saba, G.; Pinori, M.; Cappelletti, S.; Mascagni, P. Cyclic pentapeptides of chiral sequence DLDDL as scaffold for antagonism of G-protein coupled receptors: Synthesis, activity and conformational analysis by NMR and molecular dynamics of ITF 1565 a substance P inhibitor. *Biopolymers* **1999**, *50*, 211−219.
(37) Oishi, S.; Kamano, T.; Niida, A.; Odagaki, Y.; Hamanaka, N.; Yamamoto, M.; Ajito, K.; Tamamura, H.; Otaka, A.; Fujii, N. Diastereoselective synthesis of new ψ[[(*E*)-CH=CMe]- and ψ[[(*Z*)-CH=CMe]-type alkene dipeptide isosteres by organocopper reagents and application to conformationally restricted cyclic RGD peptidomimetics. *J. Org. Chem.* **2002**, *67*, 6162−6173.
(38) Tamamura, H.; Hiramatsu, K.; Kusano, S.; Terakubo, S.; Yamamoto, N.; Trent, J. O.; Wang, Z.; Peiper, S. C.; Nakashima, H.; Otaka, A.; Fujii, N. Synthesis of potent CXCR4 inhibitors possessing low cytotoxicity and improved biostability based on T140 derivatives. *Org. Biomol. Chem.* **2003**, *1*, 3656−3662.
(39) Tamamura, H.; Hiramatsu, K.; Mizumoto, M.; Ueda, S.; Kusano, S.; Terakubo, S.; Akamatsu, M.; Yamamoto, N.; Trent, J. O.; Wang, Z.; Peiper, S. C.; Nakashima, H.; Otaka, A.; Fujii, N. Enhancement of the T140-based pharmacophores leads to the development of more potent and bio-stable CXCR4 antagonists. *Org. Biomol. Chem.* **2003**, *1*, 3663−3669.
(40) Inagawa, J.; Ishikawa, M.; Yamaguchi, M. A mild and convenient method for the reduction of organic halides by using a SmI_2-THF solution in the presence of hexamethylphosphoric triamide (HMPA). *Chem. Lett.* **1987**, 1485−1486.
(41) Otaka, A.; Yukimasa, A.; Watanabe, J.; Sasaki, Y.; Oishi, S.; Tamamura, H.; Fujii, N. Application of samarium diiodide (SmI_2)-induced reduction of γ-acetoxy-α,β-enoates with α-specific kinetic electrophilic trapping for the synthesis of amino acid derivatives. *Chem. Commun.* **2003**, 1834−1835.
(42) Fukuyama, T.; Jow, C. K.; Cheng, M. 2- and 4-nitrobenzenesulfonamides: exceptionally versatile means for preparation of secondary amines and protection of amines. *Tetrahedron Lett.* **1995**, *36*, 6373−6374.
(43) Maligres, P. E.; See, M. M.; Askin, D.; Reider, P. J. Nosylaziridines: activated aziridine electrophiles. *Tetrahedron Lett.* **1997**, *38*, 5253−5256.
(44) Mitsunobu, O. The use of diethyl azodicarboxylate and triphenylphosphine in synthesis and transformation of natural products. *Synthesis* **1981**, *1*, 1−28.
(45) Blanchette, M. A.; Choy, W.; Davis, J. T.; Essenfeld, A. P.; Masamune, S.; Roush, R. W.; Sakai, T. Horner-Wadsworth-Emmons reaction: Use of lithium chloride and an amine for base-sensitive compounds. *Tetrahedron Lett.* **1984**, *25*, 2183−2186.
(46) Abdel-Magid, A. F.; Maryanoff, C. A.; Carson, K. G. Reductive amination of aldehydes and ketones by using sodium triacetoxyborohydride. *Tetrahedron Lett.* **1990**, *31*, 5595−5598.
(47) Honzl, J.; Rudinger, J. Amino acids and peptides. XXXIII. Nitrosyl chloride and butyl nitrite as reagents in peptide synthesis by the azide method; suppression of amide formation. *Collect. Czech. Chem. Commun.* **1961**, *26*, 2333−2344.
(48) Nakashima, H.; Masuda, M.; Murakami, T.; Koyanagi, Y.; Matsumoto, A.; Fujii, N.; Yamamoto, N. Anti-human immunodeficiency virus activity of a novel synthetic peptide, T22 ([Tyr-5, 12, Lys-7]polyphemusin II): a possible inhibitor of virus-cell fusion. *Antimicrob. Agents Chemother.* **1992**, *36*, 1249−1255.
(49) Navenot, J. M.; Wang, Z. X.; Trent, J. O.; Murray, J. L.; Hu, Q. X.; DeLeeuw, L.; Moore, P. S.; Chang, Y.; Peiper, S. C. Molecular anatomy of CCR5 engagement by physiologic and viral chemokines and HIV-1 envelope glycoproteins: Differences in primary structural requirements for RANTES, MIP-1α, and vMIP-II binding. *J. Mol. Biol.* **2001**, *313*, 1181−1193.
(50) Intramolecular hydrogen bonds were not observed in the calculated structure. Thus, the EADI-containing pseudopeptides, which are discussed in this study, do not seem to exist in a characteristic turn conformation such as a βII′γ turn as reported in several papers concerning normal cyclic pentapeptides, see Nikiforovich, G. V.; Kover, K. E.; Zhang, W.-J.; Marshall, G. R. Cyclopentapeptides as flexible conformational templates. *J. Am. Chem. Soc.* **2000**, *122*, 3262−3273.
(51) Miyamoto, K.; Nakagawa, T.; Kuroda, Y. Solution structure of the cytoplasmic linker between domain III−S6 and domain IV−S1 (III−IV linker) of the rat brain sodium channel in SDS micelles. *Biopolymers* **2001**, *59*, 380−393.
(52) Ludvigsen, S.; Andersen, K. V.; Poulsen, F. M. Accurate measurements of coupling-constants from 2-dimensional nuclear-magnetic-resonance spectra of proteins and determination of φ-angles *J. Mol. Biol.* **1991**, *217*, 731−736.

JM049429H

nature
immunology

Germinal center dark and light zone organization is mediated by CXCR4 and CXCR5

Christopher D C Allen[1], K Mark Ansel[1,3], Caroline Low[1], Robin Lesley[1], Hirokazu Tamamura[2], Nobutaka Fujii[2] & Jason G Cyster[1]

Germinal center (GC) dark and light zones segregate cells undergoing somatic hypermutation and antigen-driven selection, respectively, yet the factors guiding this organization are unknown. We report here that GC organization was absent from mice deficient in the chemokine receptor CXCR4. Centroblasts had high expression of CXCR4 and GC B cells migrated toward the CXCR4 ligand SDF-1 (CXCL12), which was more abundant in the dark zone than in the light zone. CXCR4-deficient cells were excluded from the dark zone in the context of a wild-type GC. These findings establish that GC organization depends on sorting of centroblasts by CXCR4 into the dark zone. In contrast, CXCR5 helped direct cells to the light zone and deficiency in CXCL13 was associated with aberrant light zone localization.

The organization of the germinal center (GC) was described over 70 years ago based on the observation that GCs have two distinct poles or zones, called the dark and light zones based on their histological appearance[1]. These histological differences are now known to be associated with important functional differences. B cells in the dark zone, called centroblasts, undergo rounds of rapid proliferation and somatic hypermutation of their antibody variable genes. The centroblasts then become smaller, nondividing centrocytes and undergo selection in the light zone based on the affinity of their surface antibody for the inducing antigen[2]. In addition to centrocytes, the light zone contains helper T cells and a network of follicular dendritic cells (FDCs) that sequester antigen[2,3]. Centrocytes that fail to bind sufficient antigen or to receive T cell help undergo apoptotic cell death and are cleared from the GC by macrophages with tingible bodies (cellular debris)[2], whereas centrocytes that successfully bind antigen and receive T cell help survive and exit the GC as long-lived plasma cells or memory B cells[2–5].

GCs develop in a stereotypic way in B cell follicles during the first week of T cell–dependent immune responses. After an initial period of rapid B cell proliferation in the follicle, the dark zone develops proximal to the T cell zone or medullary cord region and the light zone emerges at the distal pole[6]. Once these zones are established, the proliferating centroblasts in the dark zone continuously renew the centrocytes in the light zone. Evidence for the movement of proliferating cells from the dark zone to the light zone has been provided by kinetic analyses of cells labeled with [^{3}H]thymidine or 5-bromo-2′-deoxyuridine (BrdU)[2,6,7]. Data also suggest that selected centrocytes can return to the dark zone for further rounds of division and somatic mutation[3].

Despite the extensive anatomical description of GC dark and light zones and the evidence that B cells move between these compartments, the mechanisms responsible for achieving this polarity in the GC remain a mystery. The adhesion molecules ICAM-1 and VCAM-1 are reportedly expressed in the GC and can mediate attachment of GC B cells to FDCs *in vitro* via the integrins LFA-1 and VLA-4 (refs. 8,9), but there is no evidence so far for their *in vivo* involvement in GC organization. Mice lacking the chemokine CXCL13 (BLC or BCA-1) or its receptor, CXCR5, show defects in GC size and position[10–12], but it has been unclear whether these defects are secondary to the failure of these mice to develop primary follicles and FDCs or whether they reflect a function for CXCL13 in the GC. The chemokine receptor CXCR4 is expressed on human and mouse GC B cells[13–17] and on human GC T cells[18]. However, in *in vitro* studies[13,15,17,19], GC B cells have demonstrated poor chemotactic responses to the only known CXCR4 ligand, SDF-1 (CXCL12), leading some to conclude that GC B cells have an intrinsic lack of motility.

Here we have explored the mechanisms responsible for GC organization. We demonstrate using genetic and pharmacological approaches that CXCR4 is essential for GC dark and light zone segregation. When GC B cells were rescued from rapid *in vitro* apoptosis by overexpression of the antiapoptotic Bcl-2, they showed robust chemotactic responses to SDF-1 and CXCL13. SDF-1 was expressed in GCs and was in higher abundance in the dark zone than in the light zone. Furthermore, CXCR4 more abundant centroblasts than on centrocytes and was required for centroblast localization in the dark zone. In contrast, CXCR5 helped direct cells to the CXCL13-positive light zone but it was not essential for light and dark zone segregation. However, CXCL13 and CXCR5 were

[1]Howard Hughes Medical Institute and Department of Microbiology and Immunology, University of California San Francisco, San Francisco, California 94143-0414, USA. [2]Graduate School of Pharmaceutical Sciences, Kyoto University, Sakyo-ku, Kyoto 606-8501, Japan. [3]Present address: Center for Blood Research, Harvard Medical School, 200 Longwood Avenue, Boston, Massachusetts 02115, USA. Correspondence should be addressed to J.G.C. (cyster@itsa.ucsf.edu).

Published online 1 August 2004; corrected 8 August 2004 (details online); doi:10.1038/ni1100

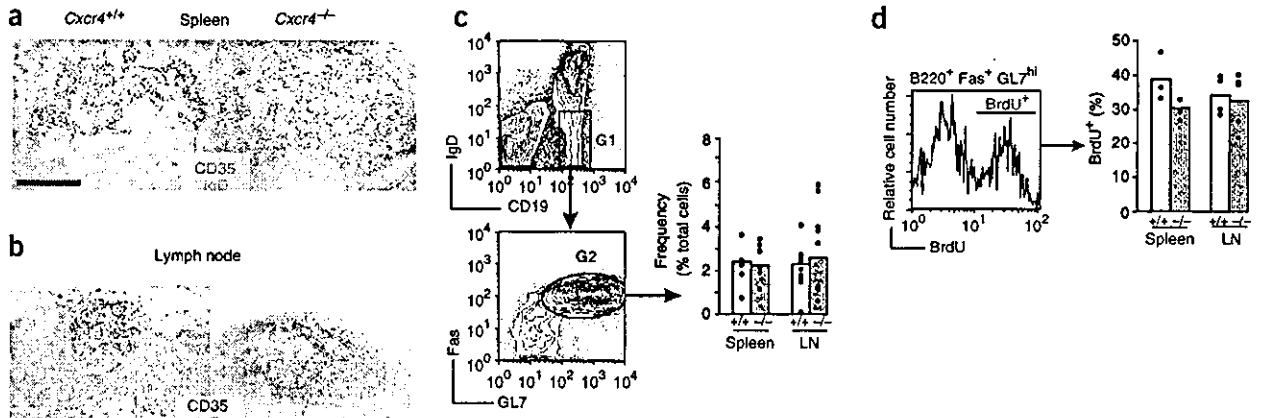

Figure 1 CXCR4 deficiency results in GC disorganization. (**a**) Immunohistochemistry of spleen GCs from immunized *Cxcr4*$^{+/+}$ or *Cxcr4*$^{-/-}$ fetal liver chimeras. Cryostat sections were stained with anti-CD35 (blue) to show the FDC network and with anti-IgD (brown) to show the IgD$^-$ GC surrounded by the IgD$^+$ follicular mantle zone. Each image is representative of GCs analyzed in four chimeras in two independent experiments. Scale bar, 100 μm. (**b**) Immunohistochemistry of lymph node GCs from immunized *Cxcr4*$^{+/+}$ or *Cxcr4*$^{-/-}$ fetal liver chimeras after 5 h of *in vivo* labeling with BrdU. Cryostat sections were stained with anti-IgD (brown) to show the surrounding follicular mantle zone; anti-CD35, FDC-M2 and anti-CD23 (all blue) for detection of the FDC network; anti-CD3 (blue) for detection of T cells; and anti-BrdU (red) for detection of proliferating centroblasts that had incorporated BrdU. Serial sections are of a single GC and are representative of GCs analyzed in three to six draining lymph nodes each from eight (CD35 and CD23), four (BrdU) or two (FDC-M2) chimeras of each type. Scale bar, 100 μm. (**c**) GC B cell frequency as percent of total organ cells, by flow cytometry. Left, GC B cells were identified as CD19$^+$IgD$^-$ cells (red box, G1) that were also GL7^{hi}Fas$^+$ (red oval, G2). Flow cytometry profiles are presented as 5% probability contour plots. In a minority of experiments, GC B cells were identified as B220$^+$GL7^{hi}PI$^-$ cells; these gating 'schemes' gave similar frequencies. Right, frequency of GC B cells as a percentage of total cells. Bars show mean and dots, individual data points. (**d**) Frequency of BrdU$^+$ GC B cells determined by flow cytometry after 5 h of *in vivo* labeling with BrdU. Red line (left) indicates BrdU$^+$ cells. Right, bars represent mean and dots, individual data points. For **c** and **d**, data points represent individual chimeras from two to three experiments. +/+, *Cxcr4*$^{+/+}$; −/−, *Cxcr4*$^{-/-}$; LN, lymph node.

required for determination of the correct position of the light zone in the GC.

RESULTS

CXCR4 is required for dark and light zone segregation

To determine whether CXCR4 is required for GC organization, we generated fetal liver chimeras by transferring wild-type (*Cxcr4*$^{+/+}$) or *Cxcr4*$^{-/-}$ fetal liver cells into lethally irradiated recipient mice. After reconstitution, we immunized these chimeras intraperitoneally with sheep red blood cells (SRBCs), a strong GC-inducing antigen, and analyzed the spleens 8 d later, at the peak of the GC response[20]. To visualize the dark and light zones of each GC, we analyzed by immunohistochemistry several cross-sections spanning more than 200 μm of depth for each spleen. In *Cxcr4*$^{+/+}$ fetal liver chimeras, GCs showed enriched staining for CD35$^+$ FDCs in the light zone, whereas in *Cxcr4*$^{-/-}$ fetal liver chimeras, GCs showed no evidence of CD35$^+$ FDC polarity; instead, the FDC network extended throughout the GC (Fig. 1a).

To assess whether this phenotype might represent a broad requirement for CXCR4 in GC organization, we immunized *Cxcr4*$^{-/-}$ and *Cxcr4*$^{+/+}$ fetal liver chimeras subcutaneously with antigen in adjuvant and then analyzed draining lymph nodes 10–14 d later. GCs in the lymph nodes of *Cxcr4*$^{-/-}$ fetal liver chimeras also showed disrupted organization, as assessed by staining the FDC network with antibody to CD35 (anti-CD35) and antibody FDC-M2 (Fig. 1b). Examination of lymph nodes also allowed us to track CD23, a marker selectively expressed on FDCs in the light zone of lymph node GCs[2,21], as seen in *Cxcr4*$^{+/+}$ fetal liver chimeras (Fig. 1b, left). In contrast, this marker was expressed throughout the GC in *Cxcr4*$^{-/-}$ fetal liver chimeras (Fig. 1b, right). In addition, the chemokine CXCL13, which is normally present in the GC light zone[22], was found throughout the GC in *Cxcr4*$^{-/-}$ fetal liver chimeras (data not shown), possibly contributing to the disrupted GC organization. These data suggest that CXCR4 is required for the formation of distinct dark and light zones.

In addition to analyzing the FDC network, we assessed the distribution of GC B cells by treating immunized chimeras with BrdU. We found that a 5-hour treatment time was optimal for preferential labeling of centroblasts in the dark zone in mouse GCs (data not shown), consistent with a previous kinetic analysis of rat GCs[6]. GCs in *Cxcr4*$^{+/+}$ fetal liver chimeras had many BrdU$^+$ cells in the dark zone and only a few labeled cells in the light zone (Fig. 1b, left), whereas GCs in *Cxcr4*$^{-/-}$ fetal liver chimeras had BrdU$^+$ cells uniformly distributed throughout the GC (Fig. 1b, right). By analyzing each GC in serial sections for the distribution of BrdU$^+$ centroblasts and CD23$^+$ FDCs, we identified dark and light zones in less than 7% of CXCR4-deficient GCs compared with more than 75% of wild-type GCs.

The requirement for CXCR4 in the GC was specific for dark and light zone segregation, as other aspects of the structure, such as size and position, were not dependent on CXCR4. Flow cytometry showed that the frequency of GC B cells was similar in *Cxcr4*$^{+/+}$ and *Cxcr4*$^{-/-}$

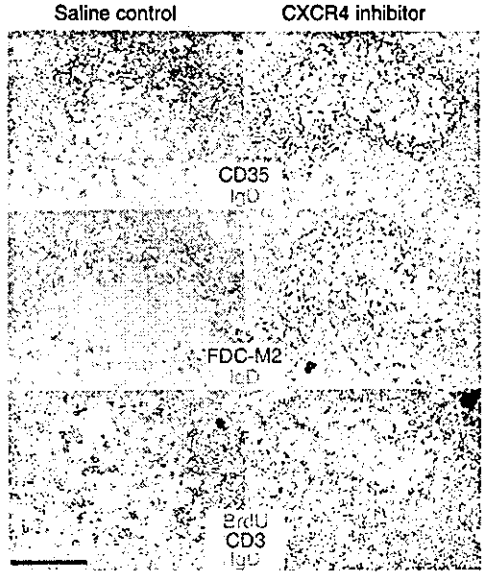

Figure 2 Treatment with a CXCR4 inhibitor results in GC disorganization. Immunohistochemistry of spleens from wild-type B6 mice immunized intraperitoneally on day 0 with SRBCs, implanted subcutaneously on day 1 with Alzet pumps containing saline (vehicle; Saline control) or the CXCR4 inhibitor 4F-benzoyl-TE14011 and analyzed 5 h after BrdU injection on day 8. Serial cryostat sections are of a single GC (antibodies used for staining, between images). Data are representative of GCs analyzed in two mice from each group. Scale bar, 100 μm.

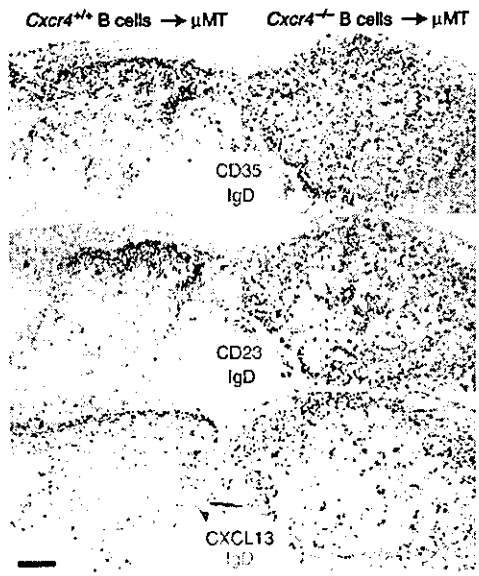

Figure 3 Deficiency of CXCR4 in B cells disrupts FDC and CXCL13 polarity in the GC. *Cxcr4*$^{+/+}$ or *Cxcr4*$^{-/-}$ B cells were purified from the spleens of fetal liver chimeras and were then transferred into B cell–deficient mice (μMT), which were immunized subcutaneously 10–11 d after transfer and analyzed 10 d after immunization. Lymph node GCs were analyzed by immunohistochemistry of cryostat sections (antibodies used for staining, between images). Serial sections are of a single GC and are representative of GCs analyzed in four mice from each group in two experiments. Scale bar, 100 μm.

fetal liver chimeras (Fig. 1c). Even when the reconstitution of B cells was poor in *Cxcr4*$^{-/-}$ fetal liver chimeras, the frequency of GC B cells was similar to that of controls (data not shown), consistent with previous reports that GC size is independent of the total number of B cells in an animal[23]. CXCR4 deficiency also did not affect the frequency of proliferating centroblasts in the GC, as determined by BrdU labeling (Fig. 1d). These findings further support the hypothesis that CXCR4 is specifically required for proper dark and light zone segregation of the GC.

To rule out the possibility that the disrupted GC organization in *Cxcr4*$^{-/-}$ fetal liver chimeras might be due to long-term defects in bone marrow development of hematopoietic cells, we administered the CXCR4 inhibitor 4F-benzoyl-TE14011 (ref. 24) to immunized normal mice for 7 d. Immunohistochemical analysis showed that GCs in these inhibitor-treated mice resembled GCs in *Cxcr4*$^{-/-}$ fetal liver chimeras. In spleen GCs, identification of centroblasts by BrdU labeling and visualization of FDCs by CD35 and FDC-M2 staining showed an absence of dark and light zone segregation (Fig. 2). Analysis of lymph node GCs by staining for CD35 and CD23 demonstrated a similar loss of GC organization after inhibitor treatment (data not shown). These results indicated that both genetic ablation and pharmacological inhibition of CXCR4 disrupted GC compartmentalization, establishing that CXCR4 is required for proper GC organization.

CXCR4 expression by B cells regulates GC organization

Although the origin of FDCs remains controversial, considerable evidence indicates that these cells are radiation resistant[22] and would therefore be wild-type in *Cxcr4*$^{-/-}$ fetal liver chimeras. To test whether expression of CXCR4 on B cells was required for GC organization, we purified B cells from *Cxcr4*$^{+/+}$ or *Cxcr4*$^{-/-}$ fetal liver chimeras and transferred them into B cell–deficient recipient mice (μMT) that we then immunized subcutaneously. Immunohistochemical analysis of the responding lymph nodes in the recipients showed that FDC and CXCL13 light zone polarity was typically absent in the GC when only B cells lacked CXCR4 (Fig. 3). To test whether expression of CXCR4 on T cells was required for GC organization, we constructed mixed irradiation chimeras by transferring a mixture of 90% T cell receptor β–deficient (*Tcrb*$^{-/-}$) *Tcrd*$^{-/-}$ bone marrow and 10% *Cxcr4*$^{-/-}$ fetal liver into recombination activating gene 1 (RAG1)–deficient *Rag1*$^{-/-}$ hosts, such that most cells would be wild-type but T cells could be derived only from the *Cxcr4*$^{-/-}$ fetal liver. In these chimeras, immunohistochemical analysis showed normal CD23 light zone polarity (data not shown). These data identify an essential function for CXCR4 on B cells but not T cells in normal GC organization and indicate that B cells regulate the position of FDCs and CXCL13 in the GC.

Enhanced chemotaxis of GC B cells to SDF-1

Human tonsil GC B cells express CXCR4 (refs. 13,15–17). Flow cytometric analysis of chemokine receptor surface expression on mouse GC B cells (Fig. 4a) showed that most GC B cells expressed 5- to 20-fold more CXCR4 than did follicular B cells. In contrast, expression of CXCR5 was similar or weakly increased (approximately twofold) and expression of CCR7, a receptor for T zone chemokines, was similar to or slightly reduced compared with that of follicular B cells (Fig. 4a). Although previous studies failed to find a substantial chemotactic response of freshly isolated GC B cells to lymphoid chemokines, including SDF-1 (refs. 13,15,17,19), it seemed possible that this was due to the propensity of isolated GC B cells to rapidly

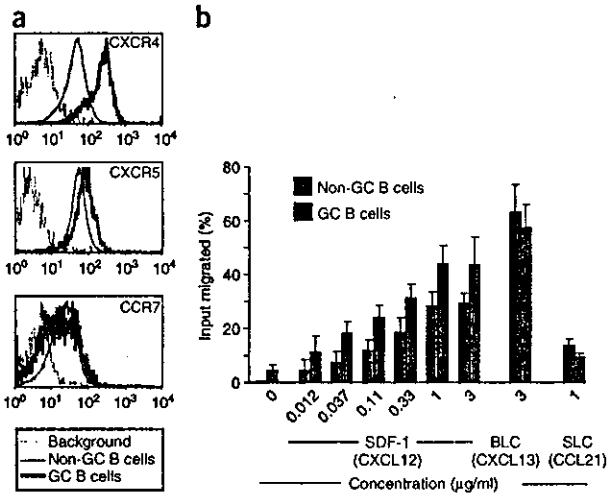

Figure 4 GC B cells upregulate CXCR4 and show enhanced chemotaxis to SDF-1. (a) Flow cytometric analysis of chemokine receptors for GC B cells, non-GC B cells or the following background controls: CXCR4, *Cxcr4*$^{-/-}$ GC B cells; CXCR5, *Cxcr4*$^{-/-}$*Cxcr5*$^{-/-}$ GC B cells; or CCR7, wild-type GC B cells stained with human LFA-3-Fc (staining control). Plots are representative of both spleen and lymph node data from the following immunized mice: CXCR4, 56 mice in twenty experiments; CXCR5, 21 mice in nine experiments; CCR7, 3 mice in three experiments. (b) Transwell migration assay of spleen cells from immunized Eμ-*Bcl2*-22 transgenic mice. Data are from four experiments with a similar overall magnitude of response and are representative of eight experiments. Bars show mean ± s.d. GC B cells show a significantly increased responsiveness to SDF-1 ($P<0.05$; 0.012–1 μg/ml) and a significantly reduced responsiveness to CCL21 ($P<0.05$) compared with non-GC B cells (Student's paired *t*-test). GC B cells were gated on a combination of the following markers: B220$^+$, CD19$^+$, GL7^{hi}, Fas$^+$ and/or IgD$^-$; non-GC B cells were gated with a combination of B220$^+$, CD19$^+$, GL7^{lo}, Fas$^-$ and/or IgD$^+$. In some experiments, dead cells were excluded by propidium iodide staining.

undergo apopotsis[2]. Indeed, in transwell migration assays with cells from immunized spleens we found that more than half of the GC B cells disappeared during the 3-hour assay, presumably by clearance mechanisms for apoptotic cells, and that the vast majority of remaining cells stained positive for annexin V and/or propidium iodide (data not shown). To overcome this rapid cell death, we used cells from mice overexpressing *Bcl2* under control of the Ig μ enhancer (Eμ-*Bcl2*-22 mice)[25]. These mice have been reported to have relatively normal GC size and morphology[26,27], and our analysis of GCs in spleens from immunized and BrdU-labeled Eμ-*Bcl2*-22 mice showed distinct centroblast and FDC clusters, consistent with normal dark and light zone segregation (Supplementary Fig. 1 online). In transwell migration assays, transgenic *Bcl2* expression reduced the frequency of apoptotic GC B cells to less than 20% (data not shown). In contrast with previous findings, *Bcl2*-transgenic GC B cells showed enhanced migration to SDF-1 relative to that of follicular B cells, whereas migration to CXCL13 was similar and migration to a CCR7 ligand, CCL21 (SLC), was modestly reduced (Fig. 4b). Therefore, of the lymphoid chemokines and receptors, GC B cells have increased responsiveness to SDF-1 and increased surface expression of CXCR4, providing a further indication of involvement of this chemokine-receptor pair in the GC.

SDF-1 expression in the dark zone

SDF-1 mRNA expression has been detected by *in situ* hybridization in the splenic red pulp[28] and lymph node medullary cords[28] and in cells associated with high endothelial venules[29], but not in the GC[15,28]. Immunohistochemical analysis with two polyclonal SDF-1 antibodies showed a similar distribution of SDF-1 protein but failed to detect SDF-1 in the GC (data not shown), consistent with two previous reports that SDF-1 protein was not detected in human tonsil and lymph node GCs[30,31]. However, as the findings reported above provided strong functional evidence that SDF-1 was present in GCs, we tested whether another reagent, the monoclonal antibody K15C[32], was more sensitive in detecting SDF-1 than were the polyclonal reagents. Because K15C is a mouse antibody, we analyzed SDF-1 expression in lymphoid tissue from immunized rats. K15C produced staining that was more intense in lymph node medullary cords and high endothelial venules than did the polyclonal reagents and also

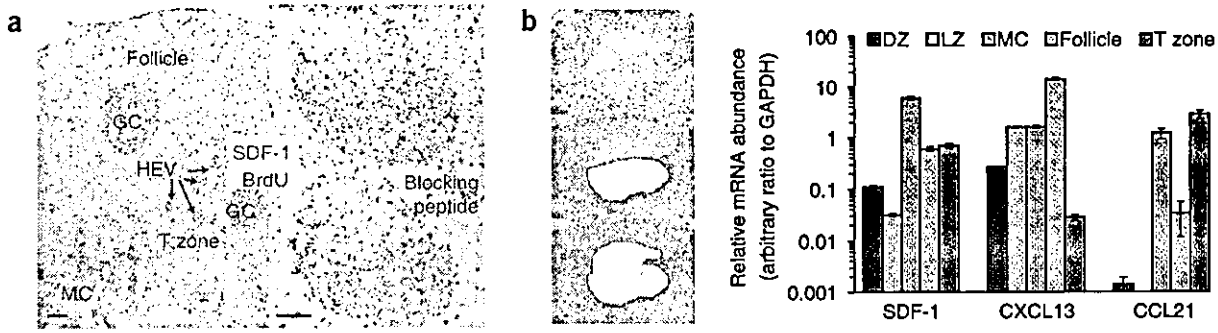

Figure 5 Detection of SDF-1 protein and mRNA in the GC. (a) Representative immunohistochemistry of cryostat sections of immunized rat lymph nodes stained with anti-BrdU (blue) and K15C anti-SDF-1 (red) with or without the blocking peptide. Left, low-power view; the GCs are not polarized in this plane of view. Right, serial cryostat sections in which a GC has dark and light zone polarity, as identified by BrdU labeling of centroblasts in the dark zone. Data are representative of two experiments with tissue from three rats. Scale bars, 100 μm. (b) Analysis of SDF-1 mRNA expression by laser-capture microdissection and quantitative RT-PCR. Top left, GC dark and light zones identified in immunized mouse lymph nodes by the respective density of methyl green staining, in which the dense cluster of large centroblasts in the dark zone produces darker staining than the loosely associated, smaller centrocytes in the light zone. Middle and bottom left, representative laser-capture microdissection (captured regions, white) of a dark zone (middle) and light zone (bottom). Right, quantitative RT-PCR analysis of mRNA expression in triplicate from one experiment (mean ± s.d.). Similar data for SDF-1 and CXCL13 were obtained in three experiments (two experiments for the T zone). HEV, high endothelial venule; MC, medullary cord; DZ, dark zone; LZ, light zone.

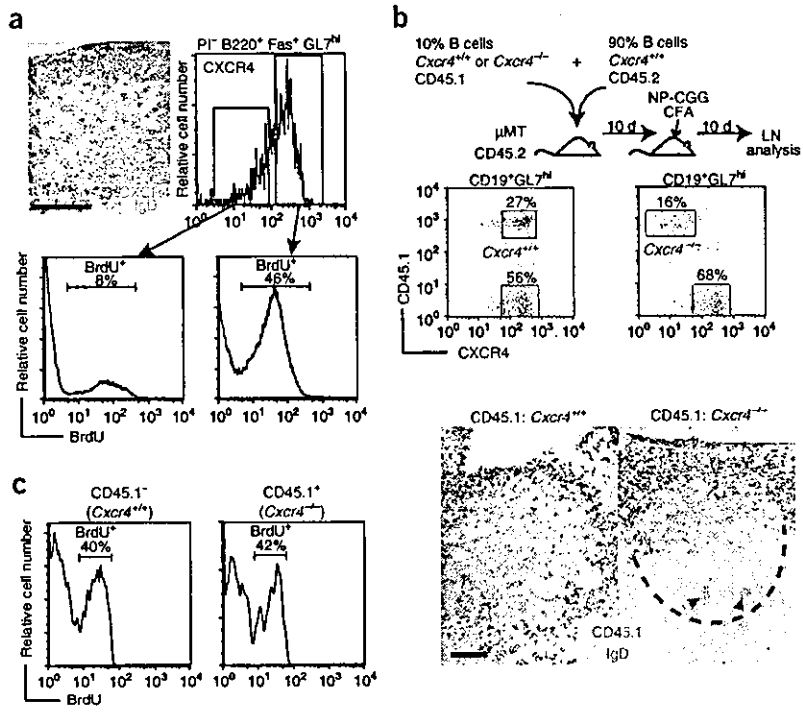

Figure 6 CXCR4 is upregulated on centroblasts and is required for dark zone localization. (a) CXCR4 is expressed in the dark zone by proliferating centroblasts. Top left, immunohistochemistry of a cryostat section of an immunized mouse lymph node (antibodies used for staining, bottom right), representative of four experiments. No CXCR4 staining was seen in the lymph nodes of *Cxcr4*$^{-/-}$ fetal liver chimeras (data not shown). Histograms: GC B cells (propidium iodide–negative, B220^{+}Fas^{+}GL7^{hi}) were sorted into CXCR4^{lo} and CXCR4^{hi} subsets after 5 h of *in vivo* labeling with BrdU, then were permeabilized and analyzed by flow cytometry for determination of the percentage of BrdU^{+} cells (numbers above bracketed lines). Cells were sorted from the spleens of six immunized mice; data are representative of two experiments. (b) CXCR4 is required for centroblasts to localize to the dark zone. For visualization of the position of *Cxcr4*$^{-/-}$ B cells in a wild-type GC, a mixture of CD45.1 (*Cxcr4*$^{+/+}$ or *Cxcr4*$^{-/-}$) and CD45.2 (*Cxcr4*$^{+/+}$) B cells were transferred into B cell–deficient mice (μMT). Flow cytometry (middle) shows the actual percentage of GC B cells (CD19^{+}GL7^{hi}) that were CD45.1^{+} in the responding lymph nodes (numbers above boxed areas, percentage of cells CD45.1^{+} or CD45.1^{-}). Bottom, the position of CD45.1^{+} cells in each GC, assessed by immunohistochemistry. The boundaries of the GCs (right, dashed lines) were determined by staining of adjacent sections with GL7 and anti-IgD (data not shown). For additional visualization of the GC region, arrowheads identify some tingible body macrophages found in the GC. Representative of five GCs each from a set of transfers. The same result was obtained in two additional experiments with mixed fetal liver chimeras. Scale bars (a,b), 100 μm. (c) Flow cytometry of the frequency of BrdU^{+} GC B cells in the mesenteric lymph nodes of a mixed chimera (CD45.1 *Cxcr4*$^{-/-}$ fetal liver and CD45.2 *Cxcr4*$^{+/+}$ bone marrow) that was immunized intraperitoneally and pulsed with BrdU. Histograms were gated on B220^{+}GL7^{hi} and CD45.1^{+} or CD45.1^{-} cells. Numbers above bracketed lines indicate percentage of BrdU^{+} cells. Data are representative of four chimeras in two experiments.

showed reactivity in T cell zones and B cell follicles (Fig. 5a, left). Moreover, K15C staining was detected in GCs, and when GC dark and light zones could be delineated distinctly by BrdU staining, the K15C signal was more intense in the dark zone than in the light zone (Fig. 5a, top right). We confirmed staining specificity by analyzing adjacent sections incubated with K15C in the presence of an SDF-1 peptide that encompasses the K15C epitope (thus, it acts as a blocking peptide; Fig. 5a, bottom right). These observations prompted us to further test whether SDF-1 mRNA could be detected in GCs. For this purpose we used laser-capture microdissection to isolate dark and light zones as well as neighboring compartments from sections of mouse lymph nodes (Fig. 5b). Quantitative RT-PCR analysis of RNA prepared from the captured tissue fragments showed that although the abundance was low, SDF-1 mRNA was present in the GC, with higher expression in the dark zone than in the light zone (Fig. 5b). SDF-1 mRNA expression in the follicle and T zone was similar and higher than in the GC and the highest expression was in medullary cords (Fig. 5b), an overall pattern that was similar to the K15C staining for SDF-1 protein. In contrast, CXCL13 mRNA was present in higher amounts in the light zone than the dark zone and was most abundant in follicles, consistent with previous *in situ* hybridization studies[22]. Transcripts for the T zone chemokine CCL21 were readily detected in tissue fragments isolated from the T zone but were almost undetectable in the GC dark and light zones (Fig. 5b). These findings demonstrate that SDF-1 is expressed in the GC and is present in higher amounts in the dark zone than in the light zone.

Dark zone localization is dependent on CXCR4

Based on our findings regarding SDF-1 distribution, we reasoned that CXCR4 might function to promote centroblast localization in the dark zone. Immunohistochemical analysis showed that CXCR4 expression was higher in the dark zone than in the light zone (Fig. 6a), suggesting that CXCR4 was specifically upregulated on centroblasts. We confirmed this finding by labeling proliferating centroblasts *in vivo* with BrdU, then separating CXCR4^{lo} and CXCR4^{hi} subsets of GC B cells by fluorescence-activated cell sorting (Fig. 6a) and analyzing the subsets by flow cytometry to determine the percentage of BrdU^{+} cells. The CXCR4^{hi} subset was enriched for the BrdU^{+} cells compared with the CXCR4^{lo} subset. Therefore, high CXCR4 expression correlates with the centroblast stage of GC B cell maturation.

The observation that CXCR4 expression was higher on centroblasts than on centrocytes was consistent with the hypothesis that SDF-1 is involved in positioning centroblasts in the dark zone. To further probe this possibility, we examined the position of *Cxcr4*$^{-/-}$ GC B cells in the context of a wild-type GC. We transferred purified *Cxcr4*$^{-/-}$ or *Cxcr4*$^{+/+}$ B cells expressing the congenic marker CD45.1 together with *Cxcr4*$^{+/+}$ CD45.2 cells into B cell–deficient mice, at a ratio such that most cells were *Cxcr4*$^{+/+}$ (Fig. 6b). After immunization, immunohistochemical analysis showed that CD45.1^{+} *Cxcr4*$^{-/-}$ B cells accumulated in the light zones of wild-type GCs (Fig. 6b, right) but were absent from the dark zone, whereas CD45.1^{+} *Cxcr4*$^{+/+}$ B cells in control recipients were evenly distributed in dark and light zones, as expected (Fig. 6b, left). *Cxcr4*$^{-/-}$ B cells were also absent from the dark zone of wild-type GCs in mixed chimeras generated by mixing of

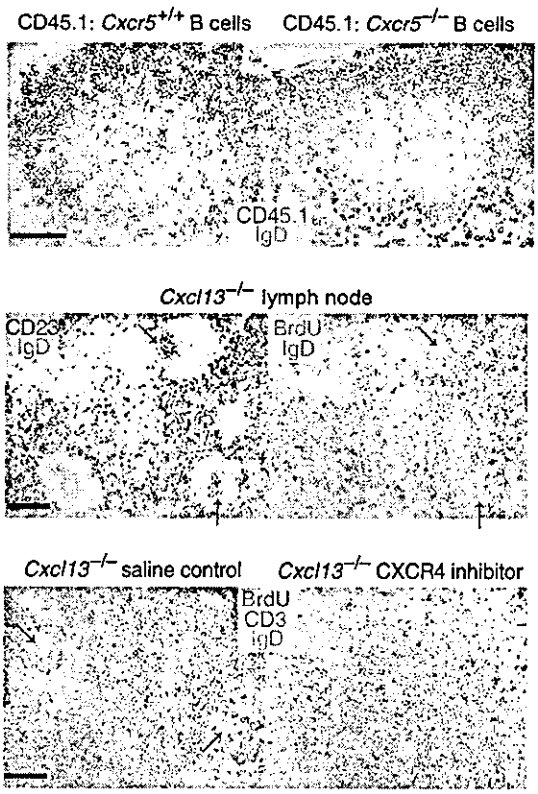

Figure 7 CXCR5 and CXCL13 function in determining light zone position. **(a)** CXCR5-deficient B cells fail to localize in the light zone of mainly wild-type GCs. A mixture of purified B cells (10% CD45.1 *Cxcr5*$^{+/+}$ plus 90% CD45.2 *Cxcr5*$^{+/+}$, or 50% CD45.1 *Cxcr5*$^{-/-}$ plus 50% CD45.2 *Cxcr5*$^{+/+}$) was transferred into B cell–deficient mice, which were then immunized and analyzed by immunohistochemistry as described in **Figure 6b**. The boundary of the dark zone (dashed lines) was identified in serial sections by staining with anti-IgD and either GL7 or anti-BrdU (data not shown). Similar GCs were noted in at least six recipients of each type in four experiments. **(b)** GCs in *Cxcl13*$^{-/-}$ mice have aberrant light zone position. GCs were analyzed by immunohistochemistry (antibodies used for staining, top left corners) of serial cryostat sections of lymph nodes present in immunized and BrdU-pulsed *Cxcl13*$^{-/-}$ mice (typically superficial cervical and mesenteric). There is dense CD23 and BrdU staining in opposing regions in two GCs. Arrows indicate the variable position of the light zone. Representative of GCs analyzed from at least three lymph nodes each from seven mice in two experiments. **(c)** CXCR4 is required for GC dark and light zone segregation in CXCL13-deficient mice. At 3 d after subcutaneous immunization, *Cxcl13*$^{-/-}$ mice were implanted with Alzet pumps containing saline (vehicle; saline control) or the CXCR4 inhibitor 4F-benzoyl-TE14011 and were analyzed on day 10 by immunohistochemistry (antibodies used for staining, between images). BrdU^{-} regions are present in some GCs after saline treatment (left; arrows) but are absent after treatment with CXCR4 inhibitor (right). Scale bars, 100 μm.

CD45.1 *Cxcr4*$^{-/-}$ fetal liver with CD45.2 *Cxcr4*$^{+/+}$ bone marrow (data not shown). BrdU labeling indicated that a similar frequency of *Cxcr4*$^{-/-}$ and *Cxcr4*$^{+/+}$ GC B cells in these mixed chimeras were undergoing cell division (**Fig. 6c**), suggesting that both *Cxcr4*$^{-/-}$ centroblasts and centrocytes were localized in the light zone. These data establish an intrinsic requirement for CXCR4 in the dark zone localization of centroblasts.

CXCR5 determines the position of dark and light zones

The GCs in mice deficient in CXCR5 or its ligand CXCL13 have reduced size and atypical distribution[10,11], yet the function of this receptor-ligand pair in the GC has been unknown. Because CXCL13 mRNA and protein were concentrated in the GC light zone[22] (**Figs. 3 and 5b**) and GC B cells were able to migrate toward CXCL13 (**Fig. 4b**), CXCL13 and CXCR5 seemed likely to direct GC B cells to the light zone. We tested this possibility by transferring a mixture of purified CD45.1 *Cxcr5*$^{-/-}$ B cells and CD45.2 *Cxcr5*$^{+/+}$ B cells into B cell–deficient recipients and analyzing the distribution of CD45.1^{+} cells in the GCs formed after immunization. *Cxcr5*$^{-/-}$ B cells were typically excluded from wild-type GCs (data not shown); however, after transferring larger numbers of these cells and analyzing many GCs, we noted that they were occasionally present in wild-type GCs. In these GCs, the *Cxcr5*$^{-/-}$ cells accumulated in the dark zone adjacent to the T zone and were absent from the light zone (**Fig. 7a**, right). These findings support the conclusion that CXCR5 and CXCL13 contribute to attracting GC B cells to the light zone.

Unexpectedly, however, immunohistochemical analysis of the small GCs that developed in the lymph nodes of immunized and BrdU-pulsed *Cxcl13*$^{-/-}$ mice demonstrated separate BrdU^{+} and CD23^{+} regions, indicating the presence of dark and light zones, in more than 66% of GCs (42 of 64; **Fig. 7b**). The relative positions of these zones were atypical, such that the light zone seemed to have a random orientation rather than being located distal to the T zone (**Fig. 7b**). Indeed, in many cases (19 of 64), CD23 staining was brightest at the center of the GC and was surrounded by a ring of BrdU^{+} centroblasts (**Fig. 7b**). We obtained similar findings by analyzing GCs in *Cxcr5*$^{-/-}$ mice (data not shown). To investigate whether CXCR4 was responsible for the segregation of dark and light zones in the absence of CXCL13 or CXCR5, we analyzed GCs in *Cxcr4*$^{-/-}$*Cxcr5*$^{-/-}$ double-deficient fetal liver chimeras and in *Cxcl13*$^{-/-}$ or *Cxcr5*$^{-/-}$ mice treated with the CXCR4 inhibitor 4F-benzoyl-TE14011. For reasons that are unclear, expression of the FDC marker CD23 was weak in the GCs that formed in either of these conditions, such that its distribution could not be assessed, making it difficult to examine dark and light zone segregation (data not shown). However, labeling with BrdU alone showed that centroblasts formed an identifiable dark zone in about 40% (23 of 61) of GCs analyzed in *Cxcl13*$^{-/-}$ or *Cxcr5*$^{-/-}$ mice, whereas less than 10% (5 of 51) of GCs showed any polarity when CXCR4 was also deficient (**Fig. 7c** and data not shown). Overall, these data suggest that CXCR4 provides a dominant cue for GC dark and light zone segregation and that CXCR5 and CXCL13 are required for the correct orientation of these zones.

DISCUSSION

The findings reported here have identified essential requirements for GC polarization into dark and light zones. GC B cells were highly motile, and centroblasts expressed more CXCR4 than did centrocytes and localized to the GC dark zone in a CXCR4-dependent way. Consistent with this CXCR4 requirement, SDF-1 was more abundant in the GC dark zone than in the GC light zone. GC B cells also expressed CXCR5 and responded to CXCL13, a chemokine present in the GC light zone, and CXCL13 and CXCR5 'dictated' the orientation of GC light and dark zones. In addition, our analysis of mice containing CXCR4-deficient B cells indicated that B cells were involved in regulating the differential distribution of FDCs in GC light and dark zones.

It has been suggested that GC B cells do not respond or respond poorly to chemokines, based on the failure of human tonsil GC B cells to migrate in *in vitro* studies[13,15,17,19]. Instead, we found that when mouse GC B cell survival was extended by *Bcl2* overexpression, these

cells showed robust migratory responses to chemokines. Consistent with an important function for SDF-1 and CXCR4 in the GC, GC B cells responded more strongly to SDF-1 and expressed more CXCR4 than did follicular B cells. In addition, the basal motility of GC B cells was higher than that of follicular B cells when examined in the absence of chemokine. A previous study of mouse Peyer's patch GC B cells also provided evidence that the cells could respond to lymphoid chemokines, although responsiveness to SDF-1 was suggested to be reduced compared with that of follicular B cells[14], a difference most likely attributable to the effects of the rapid death of unprotected GC B cells *in vitro*. Consistent with CXCR4 also functioning in human GCs, CXCR4 has been identified on human tonsil GC B cells by flow cytometry and immunofluorescence analysis of tissue sections[13,15–17]. Moreover, human follicular lymphoma cells, which are thought to be derived from GC B cells that acquire mutations promoting increased survival, show notable chemotaxis to SDF-1 (ref. 19).

Previous studies of SDF-1 distribution have failed to detect SDF-1 mRNA or protein in GCs[15,28,30,31]. By both *in situ* hybridization and analysis of protein distribution with various polyclonal anti-SDF-1 reagents, we were also unable to detect SDF-1 in GCs. However, the sensitivity of these techniques was poor and did not exclude the possibility that SDF-1 was present in GCs in low amounts. Indeed, using more sensitive approaches, we detected a broad distribution of SDF-1 mRNA and protein in lymphoid tissues, including in GCs, follicles and T zones. Although the abundance of SDF-1 in the GC was lower than in the surrounding compartments, SDF-1 amounts in the GC dark zone were higher than in the adjacent GC light zone. The overlapping SDF-1 mRNA and protein distribution indicated that the chemokine was produced locally. Because we have not detected SDF-1 mRNA in GC B cells (data not shown), we hypothesize that SDF-1 is produced by stromal cells in the dark zone. Given these findings, along with the observation that centroblasts have higher expression of CXCR4 than do centrocytes and that CXCR4 is required for GC B cells to locate in the dark zone of wild-type GCs, we conclude that SDF-1 acts to attract or retain centroblasts in the dark zone.

Despite the higher expression of SDF-1 in the follicular mantle zone than in the adjacent GC light zone, the follicular SDF-1 does not seem to reach the light zone. This suggests that SDF-1 is bound tightly at or near sites of production, a scenario that is supported by the similar profiles of SDF-1 mRNA and protein distribution throughout the lymphoid tissue. Alternatively, boundaries may exist between the GC and surrounding compartments that limit the entry of chemokines. An implication of these findings is that chemokine function can be highly localized such that adjacent tissue regions can use the same chemokine to control distinct positional events.

CXCL13 has a distribution in the GC opposite to that of SDF-1, being more abundant in the light zone than in the dark zone. Consistent with this distribution, our mixed B cell transfer experiments indicate that CXCL13 and CXCR5 function to direct B cells to the light zone. We therefore propose that as centroblasts downregulate CXCR4 and differentiate into centrocytes, the balance of chemokine responsiveness shifts in favor of CXCL13 and the cells migrate to the light zone. Unexpectedly, CXCL13 was not essential for dark and light zone segregation, as the small GCs that developed in CXCL13-deficient mice often contained both zones. However, another defect emerged in these mice: correct polarity of the GC was lost, such that the light zone was often found in the center of the GC or near the T zone. Therefore, our findings define a function for CXCL13 in promoting the positioning of the light zone in the pole of the GC distal to the T zone, and they indicate that separation of centrocytes from centroblasts is not mediated solely by migration of centrocytes to CXCL13. Instead, as dark and light zone formation continued to be CXCR4 dependent in the absence of CXCL13 (or CXCR5), it seems that differential responsiveness to SDF-1 may be sufficient to segregate centroblasts from centrocytes.

Although we have established essential functions for the CXCR4–SDF-1 and CXCR5-CXCL13 receptor-ligand pairs in the GC, our studies also lead us to propose that further guidance factors contribute to GC organization. This hypothesis is supported by the continued formation of GC clusters in mice lacking both CXCR4 and CXCL13 function. Studies done several decades ago provided evidence that transferred radiolabeled GC B cells home selectively to GCs in recipient animals[33]. As neither SDF-1 nor CXCL13 is GC specific, these observations are best explained by the existence of a GC-specific attractant. A GC-specific activity may also help keep GC cells in a tight cluster and prevent them from migrating out of the GC into the adjacent SDF-1-, CXCL13- and CCL21-rich compartments.

Although our studies demonstrate the importance of high CXCR4 expression on centroblasts, the mechanism for selective CXCR4 upregulation on these cells remains unclear. Challenging the idea of a transcriptional mechanism, a previous study showed by RNase protection assay that CXCR4 mRNA expression was similar in GC B cells and follicular B cells from immunized mouse lymph nodes[34], and using real-time PCR we have obtained similar results for sorted splenic GC B cells (data not shown). It therefore seems likely that CXCR4 is regulated in GC B cells by post-translational mechanisms. Consistent with this possibility, several modes of CXCR4 post-translational regulation have been described[35,36].

The finding that deficiency of CXCR4 specifically in B cells disrupted the organization of GC FDCs indicates that B cells are essential in GC organization. In contrast, CXCR4 deficiency in T cells was not found to disrupt GC organization, although we have not excluded the possibility of an effect of CXCR4 on T cell localization or interactions in the GC. Compared with primary follicle FDCs, GC FDCs in the light zone normally acquire additional markers, including CD23, FcγRII and VCAM-1 (refs. 2,21,22,37). Our finding that disruption of centroblast and centrocyte segregation resulted in the appearance of $CD23^+$ FDCs throughout the GC, rather than selectively in the light zone, suggests that centrocytes in the light zone normally act to promote the development of FDCs with these unique surface markers at that pole.

In conclusion, we have established that CXCR4 upregulation on centroblasts segregates these cells from centrocytes, resulting in the establishment of the GC dark and light zones. CXCL13 and CXCR5 are important in the correct positioning of these zones and contribute to recruiting cells to the light zone. The involvement of chemokines and their receptors in guiding cell movements in the GC and the high motility of GC B cells provide a basis for understanding how newly mutated GC B cells achieve efficient encounters with antigen-bearing FDCs and antigen-specific GC T cells. This study places the GC among a growing number of processes in the immune system that are dependent on CXCR4, including B cell development[38–40], T cell development[41,42], lymph node entry[29], plasma cell localization[28] and homing of neutrophils to the bone marrow[43]. The central role of CXCR4 and SDF-1 in these diverse processes supports the view that SDF-1 is a 'primordial' chemokine[44]. It also suggests another immune function that is likely to be disrupted in patients with WHIM syndrome (warts, hypogammaglobulinemia, infections and myelokathexis) who carry C-terminal truncation mutations in CXCR4 (ref. 45) and raises new concerns about the effects of global CXCR4 inhibition for antiretroviral therapy.

METHODS

Mice, rats and chimeras. C57BL/6 (B6) and B6-CD45.1 mice were obtained from The Jackson Laboratory or the National Cancer Institute. B6-SCID mice (001913; *Prkdc*^{scid}), B6-RAG mice (002216; *Rag1*^{tm1Mom}), B6-μMT mice (002288; *Igh-6*^{tm1Cgn}) and B6-TCRβδ$^{-/-}$ mice (002122; *Tcrb*$^{tm1MomTcrd^{tm1Mom}}$) were from The Jackson Laboratory and were maintained on water containing 0.25–2 mg/ml of tetracycline (Sigma-Aldrich, American Livestock Company or USB). The 129-RAG (*RAG2-M*) mice were from Taconic. *Cxcr4*$^{+/-}$ mice[40] were backcrossed at least six generations to B6 and *Cxcl13*$^{-/-}$ mice[11], *Cxcr5*$^{-/-}$ mice[12] and Eμ-*Bcl2*-22 mice[25] were backcrossed at least ten generations to the B6 strain. All mice were maintained in transgenic barrier facilities. Sprague-Dawley rats were obtained from Charles River Laboratories and were maintained in a conventional facility. Protocols were approved by the Institutional Animal Care and Use Committee of the University of California San Francisco.

Fetal liver chimeras were generated as described[28] with the following modifications: as an additional method of screening for *Cxcr4* genotype, fetal liver cells were stained with biotin-conjugated antibody to CXCR4 (anti-CXCR4) followed by fluorescein isothiocyanate (FITC)-conjugated anti-CD45.1 or anti-CD45.2, phycoerythrin-conjugated anti-B220 and streptavidin-allophycocyanin and were analyzed by flow cytometry as described below. Dead cells were excluded with 1 μg/ml of propidium iodide (Sigma-Aldrich). In most experiments, fetal liver chimeras were generated in B6-SCID, B6-RAG or 129-RAG recipients to avoid a contribution from residual host lymphocytes. B6-SCID mice were irradiated with a single dose of 400 rads and B6-RAG mice were irradiated with two doses of 450 rads. After the *Cxcr4*$^{+/-}$ mice were backcrossed more than ten generations to the B6 strain, it was necessary to increase the number of *Cxcr4*$^{-/-}$ fetal liver cells transferred to at least 5×10^6 live cells per recipient to obtain reasonable B cell reconstitution frequencies (within threefold of normal). Data include only results from chimeras that had a peripheral B cell frequency of at least 6% of total lymphocytes (average: *Cxcr4*$^{+/+}$ fetal liver chimeras, 46%; *Cxcr4*$^{-/-}$ fetal liver chimeras, 18%).

Immunizations and BrdU treatment. For induction of spleen GCs, mice were immunized intraperitoneally with SRBCs (Colorado Serum Company) as described[20] and were analyzed 8 d later. For induction of lymph node GCs, animals were immunized subcutaneously in the scruff of the neck, shoulders, flanks and/or above the tail with (4-hydroxy-3-nitrophenyl)acetyl-chicken gamma globulin (mice, total of 100–200 μg; rats, total of 1.5 mg; NP_{21}-CGG or NP_{36}-CGG; Biosearch Technologies) emulsified in complete Freund's adjuvant (Sigma-Aldrich). Draining lymph nodes (superficial cervical, axillary, brachial and inguinal) were analyzed 10–14 d later. For labeling of centroblasts, BrdU (Sigma-Aldrich) in PBS (mice, 2.5 mg; rats, 7 mg) was administered by intraperitoneal injection 5–6 h before animals were killed.

CXCR4 inhibitor treatment. Alzet osmotic pumps (7-day duration, 0.5 μl/h pumping rate; Model 1007D; Durect Corporation) were loaded with 40 mg/ml of the CXCR4 antagonist 4F-benzoyl-TE14011 (ref. 24) in saline and were implanted subcutaneously in the back according to the manufacturer's instructions. As an analgesic after surgery, 0.05–0.1 mg/kg of buprenorphine (Sigma-Aldrich) was given subcutaneously.

Flow cytometry and cell sorting. Cell suspensions were prepared from spleens and lymph nodes by mechanical disruption on 70-μm nylon cell strainers (Falcon) in RPMI 1640 medium (Cellgro) containing L-glutamine, 2% FBS (Gibco-BRL), antibiotics (50 IU/ml of penicillin and 50 μg/ml of streptomycin; Cellgro) and 10 mM HEPES (Cellgro), then were washed and kept on ice. For flow cytometry, cells were plated at a density of 5×10^5 to 1×10^6 cells per well in 96-well U-bottomed plates (Falcon), were stained for 20–60 min on ice with antibodies (**Supplementary Table 1** online) in 25 μl of PBS containing 2% FBS, 1 mM EDTA and 0.1% NaN_3, and were washed twice with 200 μl of this buffer after each step. Data were collected on a Becton Dickinson FACSCalibur and were analyzed with CellQuest Pro software (Becton Dickinson) or FlowJo software (TreeStar). CCR7 was stained with CCL19-Fc as described[28], except that binding was detected with biotin-conjugated goat anti-human IgG, Fcγ fragment specific (Jackson ImmunoResearch). Annexin V staining for apoptotic cells was with annexin V–biotin (BD Pharmingen) in buffer containing Ca^{2+} and Mg^{2+} and lacking EDTA. Biotinylated reagents were detected with streptavidin-allophycocyanin (Molecular Probes). In some cases, dead cells were excluded with 1 μg/ml of propidium iodide.

For cell sorting, cell suspensions were first prepared from spleens in HBSS (UCSF Cell Culture Facility) containing 0.5% FBS, 0.5% fatty acid–free bovine serum albumin (BSA; Calbiochem) and 200 μg/ml of DNase I from bovine pancreas (Sigma-Aldrich) and were washed. Cells at a density of 4×10^7 cells/ml were labeled for 30 min on ice with biotin-conjugated anti-CXCR4, and then erythrocytes were lysed by centrifugation at 4 °C in a solution of Tris-buffered NH_4Cl. Next, cells were labeled on ice with FITC-conjugated GL7 antibody, phycoerythrin-indotricarbocyanine (Cy7)–conjugated anti-Fas, streptavidin-allophycocyanin and allphycocyanin-Cy7–conjugated anti-B220 and were washed. Dead cells were excluded with 1 μg/ml of propidium iodide. Cells were sorted on a MoFlo (DakoCytomation).

The percentage of cells that had incorporated BrdU during DNA synthesis was determined by flow cytometry as described[46] with the following modifications: 5×10^5 Jurkat cells were added to each sample to help pellet the cells; these could be excluded during analysis based on their large scatter characteristics. For mixed chimeras, cells were stained for 1 h with biotin-conjugated anti-CD45.1. After fixation and permeabilization, cells were stained in PBS containing 0.5% Tween-20 and 2% FBS with a diluted mixture of FITC-conjugated GL7, phycoerythrin-conjugated anti-BrdU, either phycoerythrin-Cy7–conjugated anti-Fas or peridinine chlorophyll protein–conjugated anti-B220, and either allophycocyanin-conjugated anti-B220 or streptavidin-allophycocyanin, or for sorted cells that were already surface stained, with phycoerythrin-conjugated anti-BrdU only.

B cell purification and transfer. Spleens were mechanically dissociated on 70-μm nylon cell strainers or, in later experiments, were digested with collagenase and EDTA as described for dendritic cells[47], as this enzymatic digestion improved B cell recovery. Splenocytes were washed and resuspended in DMEM medium (Cellgro) containing 4.5 g/l of glucose, L-glutamine, 10% FBS, 10 mM HEPES, antibiotics and 50 μg/ml of DNase I. Non–B cells were labeled for 25 min on ice with biotin-conjugated anti-CD43 (S7; BD Pharmingen) and biotin-conjugated anti-CD11c (HL3; BD Pharmingen), then were washed and centrifuged with Tris-buffered NH_4Cl for lysis of erythrocytes, and then were labeled for 20 min on ice with streptavidin microbeads (Miltenyi Biotec). Samples were depleted of labeled cells by autoMACS (Miltenyi Biotec) according to the manufacturer's instructions, resulting in a B cell purity of at least 90%, as determined by flow cytometry. T cell contamination was less than 0.75%, although the identity of the remaining cells remained unclear (they did not stain positive for CD3, CD11c, Mac-1 or NK1.1). B cells (1.5×10^7 to 4.5×10^7 per recipient) were transferred by intravenous injection into the tail veins of B cell–deficient mice (μMT).

Immunohistochemistry. Spleens and lymph nodes were placed in Tissue-Tek optimum cutting temperature compound (Sakura), were 'snap-frozen' in dry ice and ethanol and were stored at −80°C. For immunohistochemistry, cryostat sections (7 μm in thickness) were affixed to multispot (Hendley-Essex) or Superfrost/Plus (Fisher Scientific) microscope slides, dried at 20–25 °C, fixed in cold acetone for 10 min and then dried at 20–25 °C. Slides were rehydrated in Tris-buffered saline (TBS), pH 7.6, and then were stained for 2–3 h at 20–25 °C in a humidified chamber in TBS containing 0.1% BSA (ICN), 1% normal mouse serum (Sigma-Aldrich) and a diluted mixture of two primary antibodies (**Supplementary Table 2** online). After slides were washed in TBS for 3 min with gentle agitation, sections were stained for 1–2 h as described above with secondary antibodies (**Supplementary Table 3** online). Biotinylated antibodies were detected with streptavidin–alkaline phosphatase (Jackson Immunoresearch or Vector Labs). Rat tissue was stained for 18 h at 4 °C as described above in TBS containing 0.1% BSA and 1% normal rat serum with 20 μg/ml of mouse monoclonal anti-SDF-1 (K15C[32]) with or without an eightfold molar excess (2 μg/ml) of the blocking peptide KPVSLSYRSPSRFFE (synthesized by SynPep), then was stained for 2 h at 20–25 °C with biotin-conjugated goat anti-mouse IgG, Fcγ fragment specific (Jackson ImmunoResearch), followed by incubation for 1–2 h at 20–25 °C with streptavidin–ABC–alkaline phosphatase (Vector Labs). Enzyme conjugates were developed as described[46] and slides were mounted in Crystal/Mount (Biomeda). Images were collected and processed as described[48]. For detection of cells that had incorporated BrdU in sections, slides were first stained by standard immunohistochemistry as